Fluid manipulations uncover mechanosensation for zebrafish left-right establishment during one-hour time interval

Pedro Sampaio[1*], Sara Pestana[1*], Adán Guerrero[2], Ivo A. Telley[3], David. J. Smith[4], Susana S. Lopes[1**]**

1. CEDOC, Chronic Diseases Research Centre, NOVA Medical School. Faculdade de Ciências Médicas, Universidade Nova de Lisboa, 1169-056 Lisboa, Portugal

2. Laboratorio Nacional de Microscopía Avanzada. Departamento de Genética del Desarrollo y Fisiología Molecular. Instituto de Biotecnología. Universidad Nacional Autónoma de México (UNAM). Cuernavaca, Morelos, Mexico.

3. Instituto Gulbenkian de Ciência, Fundação Calouste Gulbenkian, 2780-156 Oeiras, Portugal.

4. School of Mathematics, University of Birmingham, B15 2TT, UK; Institute for Metabolism and Systems Research, University of Birmingham, B15 2TT, UK.

* Co-first-authors

**Co-corresponding authors. Email: susana.lopes@nms.unl.pt; D.J.Smith@bham.ac.uk

Abstract

Humans and other vertebrates define body axis left-right asymmetry in the early stages of embryo development. The mechanism behind left-right establishment is not fully understood. Although it is known that the symmetry break occurs in a dedicated organ called the left-right organizer (LRO) and involves motile cilia generating fluid flow therein, it has been a matter of debate whether the process of symmetry breaking relies on a chemosensory or a mechanosensory mechanism. Novel tailored manipulations for LRO fluid extraction in living zebrafish embryos allowed us to pinpoint a decisive developmental period for breaking left-right symmetry during development. This critical time-window was narrowed to one hour and is characterized by a mild counterclockwise flow. The experimental challenge in our approach consisted of emptying the LRO of any potential fluid, abrogating simultaneously flow force and chemical determinants. Our findings revealed an unprecedented recovery capacity of the embryo to re-inflate and re-circulate the fluid inside the LRO exposing unknown properties of this transient organ. Live extraction and replacement of LRO fluid while changing dilution or viscosity demonstrated that early left-right patterning depends on fluid flow mechanics rather than on the nature of the fluid content. Our results advocate for a mechanosensory mechanism ruling left-right early development.

Teaser:

Zebrafish uses mechanosensation during one-hour time-window to initiate left-right development.

Vertebrate organisms break lateral symmetry during embryonic development and define left and right. This left-right axis is the third and final body axis to be established in the embryo and encompasses a biophysical process yet to be fully elucidated. In mouse, frogs and fish it involves fluid movement in a specialized organ called the left right organizer (LRO). In the mouse embryo, cilia driven fluid flow inside the LRO has been proposed to activate either a mechanosensory mechanism in the epithelial cells that constitute the LRO, or to transport morphogens (as dissolved molecules or carried inside extracellular vesicles) to particular locations of the LRO (Nonaka et al., 1998; McGrath et al., 2003; Tanaka et al., 2005). While the mechanism is unknown, it culminates in asymmetric left-sided calcium signalling at the node cells and a subsequent conserved Nodal pathway on the left side of the embryo (Takao et al., 2013; Mizuno et al., 2020). The endpoint of this developmental process is the asymmetric localization of internal visceral organs, such as the heart and liver.

Analysis of cilia driven LRO flow is therefore crucial to understand this initial process. The transparent embryo of zebrafish is a particularly suitable model system enabling flow visualization and subsequent scoring of organ asymmetry in the same individual. We have shown that wild-type (WT) zebrafish embryos have a stereotyped flow pattern in the LRO (known as Kupffer's vesicle or KV), exhibiting higher dorsal anterior speed (Sampaio et al., 2014). We have also demonstrated that deviations from this flow pattern due to less or shorter motile cilia, predictably generate larvae with wrong laterality outcomes, indicating a biological relevance to flow (Sampaio et al., 2014). Thus, flow dynamics and the mechanical-chemical readout are central to solving the problem of how left-right asymmetry is first established.

Particle tracking for fluid flow reconstruction and modelling have provided quantitative insight in zebrafish (Kramer-Zucker et al., 2005; Okabe et al., 2008; Sampaio et al., 2014; Smith et al., 2014; Juan et al. 2016; Ferreira et al., 2017; Tavares et al 2017, among others). Although the LRO is an organ with a limited lifetime of 7 hours, seminal work unveiled that the zebrafish Kupffer's vesicle is dispensable for left-right establishment after 10 somite stages (ss) (Essner et al., 2005). Guided by this finding, most subsequent studies have been performed at

8-10 ss, when an asymmetry in *dand5* gene expression is first detected (Lopes et al., 2010; Sampaio et al 2014; Ferreira et al., 2017, Ferreira et al., 2019). The clear reduction of *dand5* gene expression on the left side of the LRO is the first asymmetric molecular marker in left-right development, downstream of fluid flow, an event conserved across species (Marques et al., 2004; Hojo et al., 2007 and Schweickert et al., 2010).

Yuan and colleagues have shown that, as soon as zebrafish LRO cilia are formed and some start beating, at around 1 to 4 ss, intraciliary calcium oscillations (ICOs) can be registered in LRO cells (Yuan et al., 2015). These signals were reported to precede cytosolic calcium elevations that extend mostly to the left mesendodermal regions and were shown to be essential to trigger correct left-right patterning. Therefore, it is conceivable that an asymmetry in *dand5* mRNA expression, first detectable at 8 ss in zebrafish (Lopes et al. 2010), results from molecular events that significantly precede that time point. Although it is evident from pioneer studies using mouse mutants without cilia or with immotile cilia that fluid flow has a critical role in conveying a biased signal to the nearby cells (Nonaka et al., 1998; Supp et al., 1999), both the nature of the signal and its detection mechanism remain elusive. The mechanosensory hypothesis postulates that fluid flow can be mechanically sensed by cilia, through a Polycystin protein complex involving PKD1L1 and PKD2 cation channel (McGrath et al., 2003; Field et al., 2011; Yuan et al., 2015). Conversely, the chemosensory hypothesis posits that vesicular parcels or extracellular vesicles containing an unknown chemical determinant are transported by the directional fluid flow towards the left side of the mouse node (Tanaka et al., 2005). However, the existence of such morphogen has not yet been confirmed.

To address these 20 year-long-standing questions, we decided to take a step back and unequivocally determine the developmental period for left-right initiation. We envisaged that by determining the critical time-window within the 7 hours lifetime of the zebrafish LRO, we could then characterize its fluid flow and, thus, narrow down the variables that contribute to left-right establishment. Ultimately, we aimed at obtaining evidence for one or the other model for LR initiation as current scenarios fail to fully uncouple the LRO hydrodynamics from

the potential role of fluid flow in transporting vesicles or molecules with signalling properties (Cartwright et al., 2019).

The LRO is filled with fluid, but the nature of the fluid content is unknown because, so far, its minute volume, around one hundred picolitres, (Roxo-Rosa et al., 2015) prevented a detailed biochemical analysis. However, the inflation mechanism of the LRO lumen is known to be driven by the chloride channel known as cystic fibrosis transmembrane conductance regulator (CFTR) that, when impaired, predictably leads to empty LROs and left-right defects (Navis et al. 2013). Thus, it is possible to block the inflation process by using pharmacology, anti-sense technology or mutants for CFTR, without affecting cilia number or motility (Navis et al., 2013; Roxo-Rosa et al., 2015). However, manipulation with precision and higher resolution in time was lacking. To determine the time-window for LR initiation, we devised a novel assay that allows for highly controlled mechanical manipulation of the LRO fluid. We performed total fluid extractions from the LRO at different developmental time points only 30 minutes apart. After confirming that the KV was still present and able to refill, we followed the development of each embryo until organ laterality could be determined. This approach led us to narrow the time-window for symmetry breaking to one-hour, from 4 to 6 ss, corresponding to the cell rearrangement period first reported by Wang et al. (2011). During this time interval we found fluid flow to be mild but already directional. Extraction of LRO fluid at 5 ss led to 35% of embryos with both heart and liver incorrect localization. Embryos did not develop LR defects when the original KV fluid was replaced with Danieau buffer, but LR axis was perturbed when viscosity of the same buffer was increased. Altogether, our experiments suggest that fluid flow mechanics, but not the nature of fluid content, has a major role in LR initial establishment.

Results

Fluid extraction affects LR during one-hour time-window

KV fluid flow was disrupted by performing fluid extraction at each LRO developmental stage using a microscope-based micromanipulation setup connected to microfluidic actuators (Figure 1a). We envisaged that if we found

the sensitive time period, we could then investigate the properties that were necessary and sufficient to break LR. For this purpose, we extracted the liquid from the LRO lumen in embryos individually staged from 3 to 12 ss. Manipulated embryos were later characterized according to heart and liver laterality. This procedure depleted the LRO fluid transiently, disrupting the flow generated by motile cilia, while at the same time it potentially extracted any molecular signals that are present in the fluid. Controls for these experiments included confirmation that cilia number, length and anterior-posterior (A/P) distribution were not perturbed after fluid extraction at 5 ss, in fixed samples at 8 ss (Figure S1) and that number of motile / immotile cilia and their A/P distribution was not changed when evaluated by live imaging embryos at 6 ss (Figure S2).

Although most embryos recovered the procedure without LR defects (Figure 1b), some presented both heart and liver misplacements, starting with intervention at 3 ss (2/13 embryos, 15%), becoming more pronounced for intervention at 4 ss (7/26 embryos, 27%, Fisher test, p-value < 0.05) and peaking with intervention at 5 ss (14/40 embryos, 35%; Fisher test, p-value < 0.05). LR organ misplacements then became progressively non-significant from 6 ss onwards (4/27 embryos, 19%; Fisher test, p-value > 0.05; Figure 1b).

To elucidate how fluid depletion affected LR signalling we examined the expression pattern of *dand5*. It is well established that in WT embryos, zebrafish *dand5* is mainly expressed on the right side of the LRO at 8 ss (Lopes et al., 2010). Thus, we evaluated *dand5* expression pattern at 8 ss in embryos that were manipulated at 5 ss, which was the developmental stage with highest incidence of LR defects upon liquid extraction. We observed that *dand5* expression also became abnormally bilateral in 35% of the cases (6/17 embryos, Fisher test, p-value < 0.05; Figure 1c) suggesting that either lack of fluid flow or depletion of a molecular signal prevented left-sided degradation of *dand5* mRNA.

LRO recovers lumen area after fluid extraction

The lumen of manipulated LROs started to expand soon after fluid extraction (Figure S3a), indicating that the fluid secretion machinery mediated by CFTR (Navis et al., 2013; Roxo-Rosa et al., 2015) was not collaterally affected by the

manipulation procedure and was able to recover the normal fluid volume. Our observations contrasted with previous reports (Essner et al., 2005; Hojo et al., 2007) of irreversibly emptied LROs after manipulations, highlighting that the technical approach developed in this work confers minimal damage to the LRO core structure.

Gokey et al. (2016) showed that below 1300 μm^2 of KV cross-sectional area at 8 ss, LR patterning could be compromised. Therefore, a scenario where some LROs replenish better than others could explain a differential recovery, enabling the correct organ patterning in most, but not all embryos. Thus, we first investigated if there were significant differences in fluid recovery between manipulated embryos that developed LR defects from those that did not. We performed LRO fluid extraction at 5 ss and followed the recovery of the LRO cross-sectional area and fluid dynamics along development (at 6 ss, 7 ss and 8 ss). As expected, the LROs from the control group ('Sham') were larger at each sampled time point (t-test, p-value < 0.05) compared to the fluid extracted groups (Figure S3b). Further, our results showed that the LRO area was similar as well as the area change per somite (t-test, p-value > 0.05) in manipulated embryos that developed a normal organ patterning ('No Defects' group) and those that developed incorrect LR axis establishment ('Defects' group, (Figure S3b,c).

To perturb a re-inflation driven recovery we then challenged the LRO further by performing an additional fluid extraction one hour after the first intervention, at 7 ss (Figure S4). Our working hypothesis predicted more *dand5* defects with the double intervention. However, results showed a similar proportion of bilateral *dand5* expression (6/16, 37.5%) to that observed at 5 ss (comparing Figure 1c with Figure S4; Fisher test p-value > 0.05). This experiment confirmed that fluid extractions at 7 ss no longer affect LR development significantly as indicated in the first experiment (Figure 1b). To continue the investigation on a potential deficiency in flow recovery in the 'LR Defects' group after fluid extraction at 5 ss, we next assessed how fluid flow dynamics varied with time by retrospectively comparing embryos with and without LR defects.

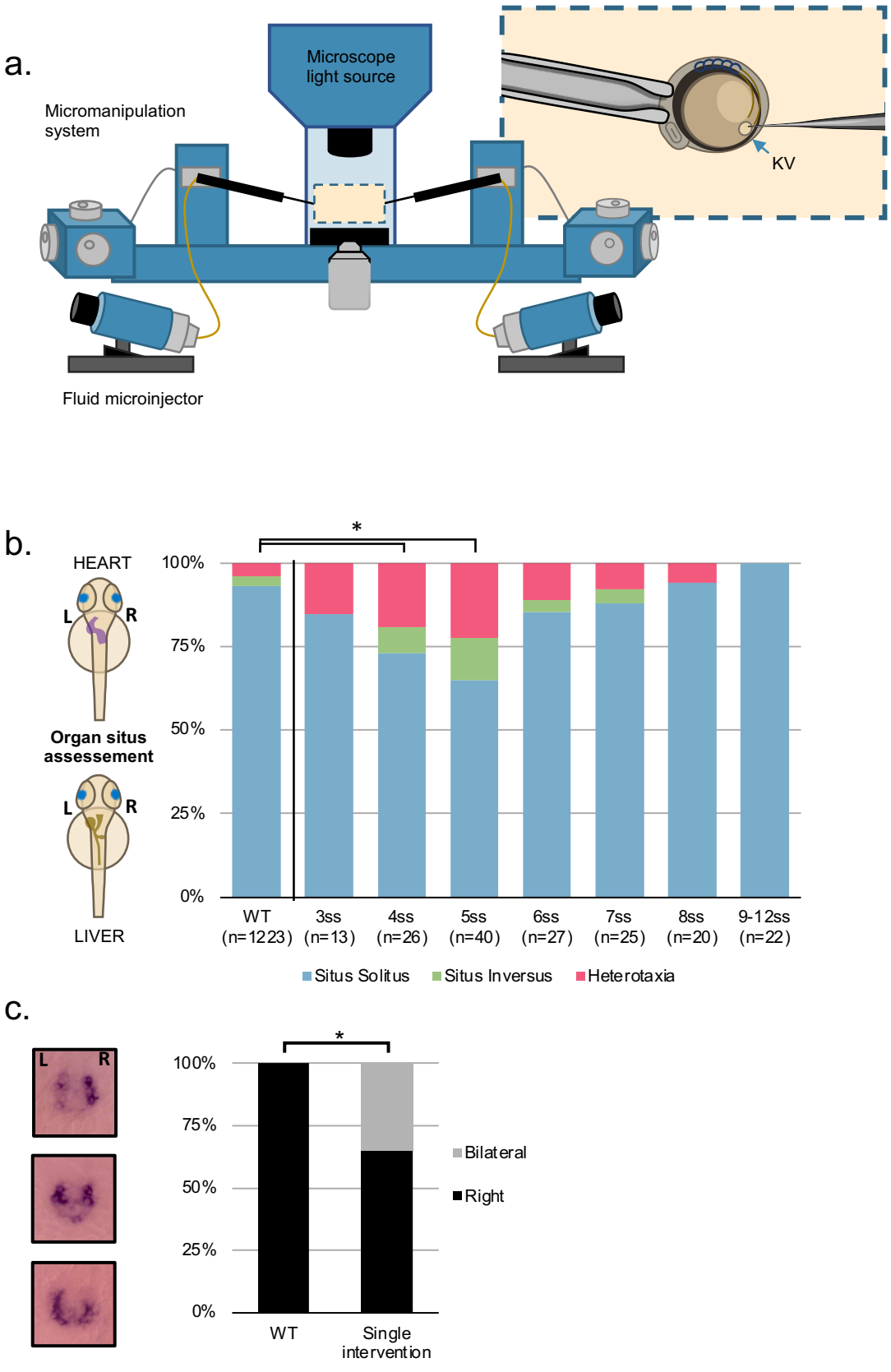

Figure 1. **Fluid extractions uncover a sensitive one-hour interval.** (a) Schematic representation on the micromanipulation setup developed for the zebrafish LRO fluid extraction throughout development. (b) Evaluation of organ patterning after 48 hours. Heart and liver position were scored for each embryo manipulated in the respective

developing stage from 3 to 12 ss, *situs inversus* in zebrafish means both organs are localized on the right side and heterotaxia means that at least one organ is wrongly localized. (c) *dand5* expression pattern after intervention for LRO liquid extraction in a subset of fixed embryos at 8 ss. LRO. left-right organizer, ss. somite stage.

Fluid flow angular velocity is reduced in manipulated embryos showing LR developmental defects

Flow can be determined by tracking particles serving as fiduciary markers. The general pattern of fluid flow in the LRO is roughly circular with local variations (Sampaio et al., 2014). Local flow speed (velocity magnitude) is a useful measure for identifying regional flow patterns, but it does not fully describe the directional material transport of the LRO fluid (Ferreira et al., 2017; Juan et al., 2018). Thus, we determined the angular velocity at discrete locations as a proxy for the circular flow speed (Figure 2a-c). Considering the two sensing hypotheses, we predicted that any type of detectable LR signal, either as flow-induced shear force or as a signalling molecule, must happen in the vicinity of the cell membrane. Taking this into consideration, we analysed the fluid dynamics within the outer half of the radius of the LRO lumen.

Angular velocity data from the many tracks obtained from each of the sham and extraction experiments were analysed at 6, 7 and 8 ss, first dividing the LRO in 8 radial sections and plotting the median angular velocity per section (Figure 2a-c). To account for the hierarchical structure of the data with both within- and between-embryo variability in angular velocity tracks, linear mixed effects models were fitted to characterise how angular velocity varied across the LRO and over time (Figure 2d-g), incorporating somite stage, normalized LR/ AP axis position and group (Sham/ Defects/ No Defects) as independent variables. Coefficient values can be interpreted as showing relative effect sizes and direction (Table S2 for p-values).

The linear mixed model for experiments with fluid extraction and ‘Sham’ intervention at 5 ss identified the following significant fixed (embryo-independent) effects: (i) a significant reduction of angular velocity in the ‘Defects group’ (p-value = 1.2e-5, coefficient -0.13 rad/s), (ii) greater angular velocity in the anterior compared with posterior region of the LRO (p-value = 6.3e-98, coefficient 0.16 rad/s), (iii) increased flow velocity over time (p-value = 7.1e-6, coefficient 0.021

rad/s/stage), (iv) enhanced left-right difference in the ‘No Defects group’ (p-value = 0.006, coefficient 0.027 rad/s), (v) reduced posterior-anterior difference in the ‘Defects group’ (p-value = 9.5e-5, coefficient -0.041 rad/s), (vi) enhanced posterior-anterior difference in the ‘No Defects group’ (p-value = 0.002, coefficient 0.034 rad/s), (vii) enhanced degree of velocity increase over time in the ’No Defects’ group (p-value = 2.3e-5, coefficient 0.027 rad/s/stage) and (viii) (at marginal significance level) some degree of velocity increase over time in the 'Defects group’ (p-value = 0.041, coefficient 0.013 rad/s/stage).

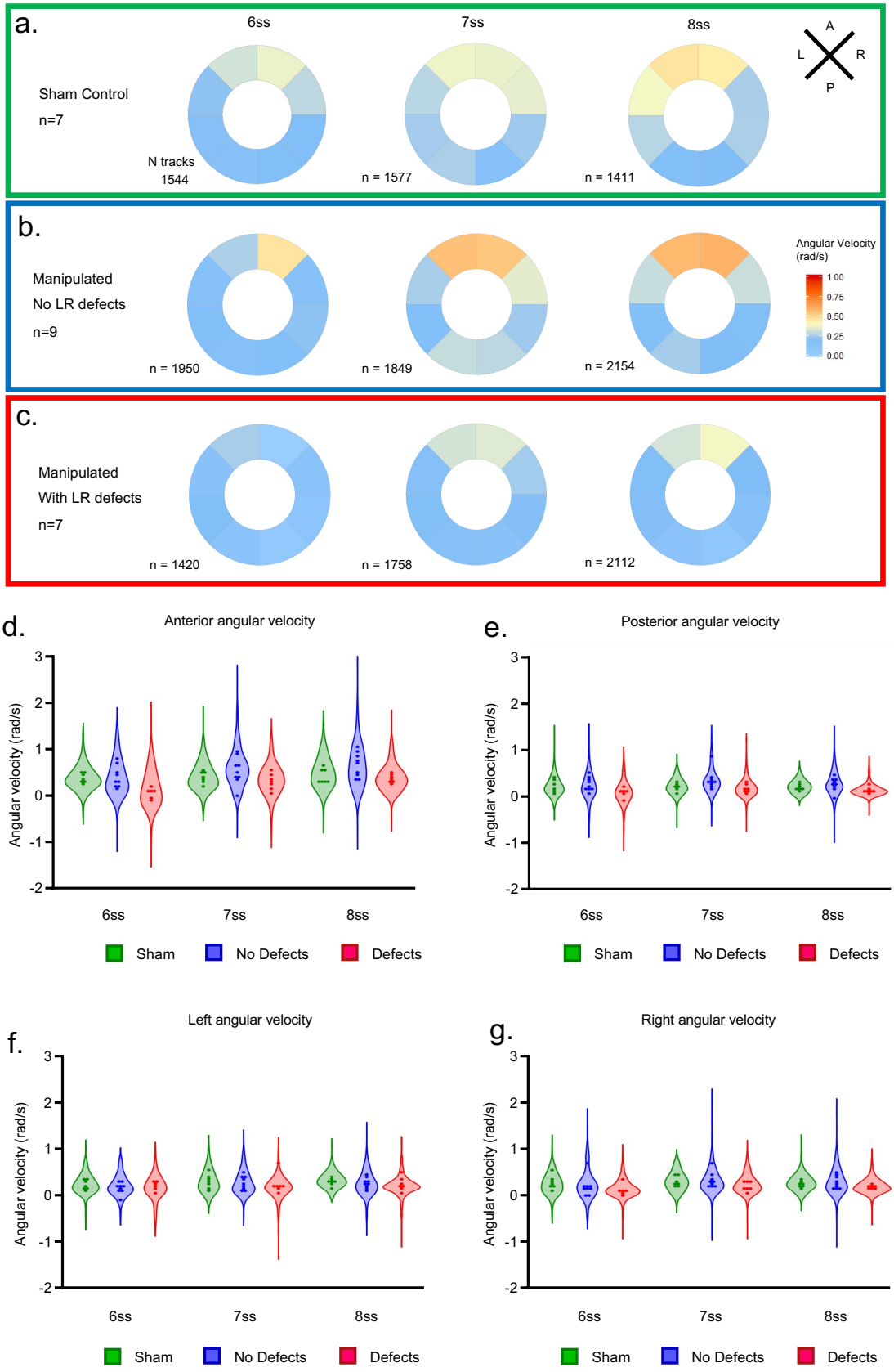

Figure 2 - **During LRO fluid flow recovery angular velocity decreases in embryos that develop left-right defects.** Angular velocity polar plots for 6 ss, 7 ss and 8 ss for the three different groups (a) “Sham” control, (b) “No LR Defects” group and (c) “With LR

Defects" group. LR defects refer to misplacement of heart or liver encountered at the larval stage after fluid extraction was performed at 5 ss; number of tracks refers to the number of particle trajectories identified for the quantifications and respective angular velocity plots. Colour code on polar plots refers to the median angular velocity for all pooled embryos. (d-g) Violin plots show quantifications and statistical comparisons of angular velocities found for all tracks analysed (d) anterior, (e) posterior, (f) left and (g) right. Dots contained in the violin plots correspond to median values per embryo. A statistical linear mixed model was applied.

Next, in order to clarify for further differences between the 'Defects' group and the other groups we investigated the directionality of the individual particles as it could provide more cues for localized differences that we observed denoted by negative values for angular velocity indicating the existence of some particles with clockwise flow. We divided the LROs into sections of 30 degrees each and by looking at the direction of each tracked particle in detail (Figures S5-S10 and Figure 3a), we only found significant differences in directionality when comparing the group 'Defects' with the 'Sham' control group in anterior sectors of the LRO at 6 ss (Figure 3b, c). In this region the 'Defects' group presented disoriented particle trajectories compared to both the 'Sham' control group and the 'No Defects' group at 6 ss (Figure S5). This suggests that the manipulation might have regionally perturbed the fluid in some embryos and that at 6 ss, the earlier time point, the effect of the transient manipulation was still detectable. Conversely, the 'No Defects' group never showed significant differences in directionality compared to the 'Sham' control group (Figure S5; see also Figure S6 to S10 for complete data on all sectors of the LRO for 7-8 ss).

In summary, our data showed that after fluid extraction at 5 ss, the group of embryos that later developed LR defects showed a decreased angular velocity, preferentially at the anterior LRO region resulting in reduced AP difference and it also presented deviations from the counterclockwise flow direction anteriorly.

This study highlighted that a relatively robust flow recovery mechanism is in place in zebrafish WT embryos, ensuring that LR succeeds in the majority of the manipulated embryos. Both groups of embryos that recovered and failed to recover LR development after the manipulation exposed new sensitive mechanical properties of the LRO flow and revealed a short time-window for LR early development.

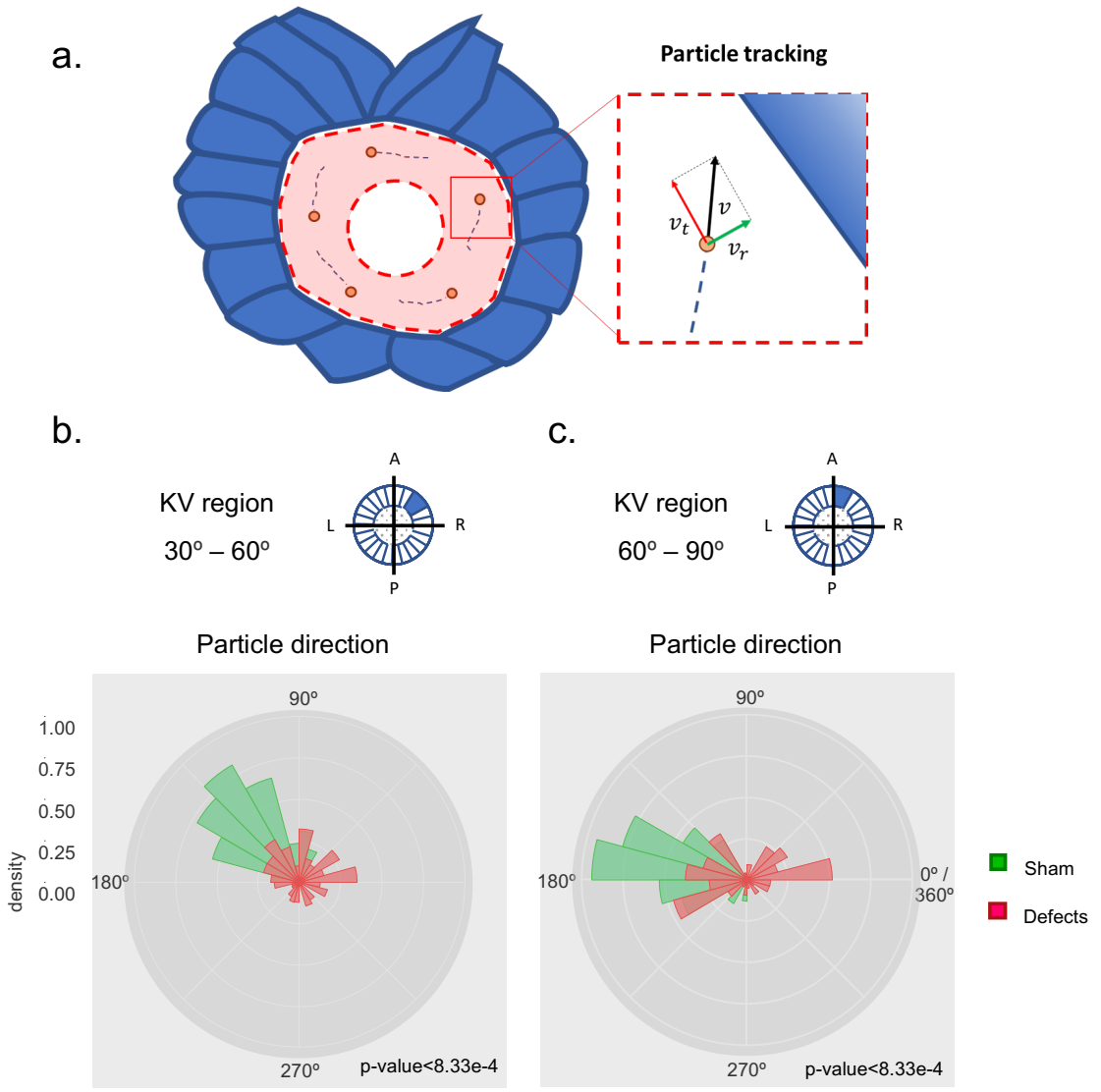

Figure 3 – **Directionality of vector fields changes in embryos that develop LR defects**. (a) Diagram representing particle directionality. LRO area sections were delimited based on intervals of 30 degrees. Highlighted are regions (b) from 30 to 60 degrees and (c) 60 to 90 degrees, that showed significant differences in particle movement between the groups 'Sham' control embryos and embryos with 'LR Defects'. Each density plot represents the pooled tracked trajectory of all moving particles at any given point in time. Respective area region analysed is represented on the top right corner of each plot. To assess differences upon fluid manipulation 'Sham' and 'Defect' groups were plotted for the 6 ss. Kolmogrov-Smirnov test was used for comparing trajectory distribution between the two groups. Full data can be found in Supplemental Figures 5-10.

A mechanosensory mechanism drives LR asymmetry

Extraction of the LRO fluid annihilated both flow dynamics and fluid content, thus it did not allow us to discern a potential mechanosensory mechanism from a

chemosensory mechanism. Benefitting from the manipulation setup we next designed an experiment that could uncouple these two sensory systems. We diluted the fluid content in a physiological buffer (Danieau buffer, DB) without changing the flow dynamics for more than a few seconds, so that we could conclude whether the fluid content was crucial for LR establishment or not. To address if this dilution experiment affected fluid content without perturbing flow dynamics, we monitored angular velocity along the recovery period and proceeded to its analysis as before. As a positive control for flow dynamics perturbation we used methylcellulose (MC, viscosity ~1500 cP; water, viscosity 1 cP) as previously used in *Xenopus* and mouse (Schweickert et al., 2007, Shinohara et al., 2012) to make the fluid more viscous. We extracted the LRO fluid from 5 ss embryos and diluted it in approximately 1µl volume of Danieau buffer (DB) previously loaded into the needle. Next, after a few seconds, we re-injected the resulting mixed liquid (Figure 4a). To test if dilution of the fluid content was indeed occurring, we performed the same experiment using a rhodamine tracer and confirmed that the LRO lumen became fluorescent after the procedure (Figure 4b). The data for median angular velocities is presented in Figure S11 and the application of a linear mixed model for this set of experiments with DB and MC dilution versus 'Sham' intervention at 5 ss identified the following significant fixed effects (Figures 4c-f; Table S3): (i) a significant reduction of angular velocity following methylcellulose (but not DB alone) dilution (p-value = 4.7e-4, coefficient -0.12 rad/s), (ii) greater velocity in the anterior compared to the posterior region of the LRO (p-value = 4.4e-142, coefficient 0.16 rad/s), (iii) increased flow velocity over time (p-value = 5.6e-8, coefficient 0.021 rad/s/stage), (iv) faster flow on the right compared with the left following MC dilution (but not DB alone) (p-value = 0.0039, coefficient 0.026 rad/s), (v) greater difference in flow between anterior and posterior following DB dilution (p-value = 0.0072, coefficient -0.021 rad/s), (vi) less difference in flow between anterior and posterior following MC dilution (p-value = 5.5e-14, coefficient -0.073 rad/s), and (vii) (at the significance level of 0.01) there is some evidence for any positive effect of DB dilution (e.g. in the anterior) receding over time (p-value = 0.010, coefficient -0.013 rad/s/stage).

Remarkably, we observed that dilution of LRO fluid with MC significantly reduced cilia beat frequency (31.17 Hz ± 1.4; n = 50 cilia, 5 embryos) as compared to ‘Sham’ controls (39.29 Hz ± 1.2 n = 55 cilia; 5 embryos; Figure 4g, Student’s t-test with Welch’s correction, p-value < 0.01).

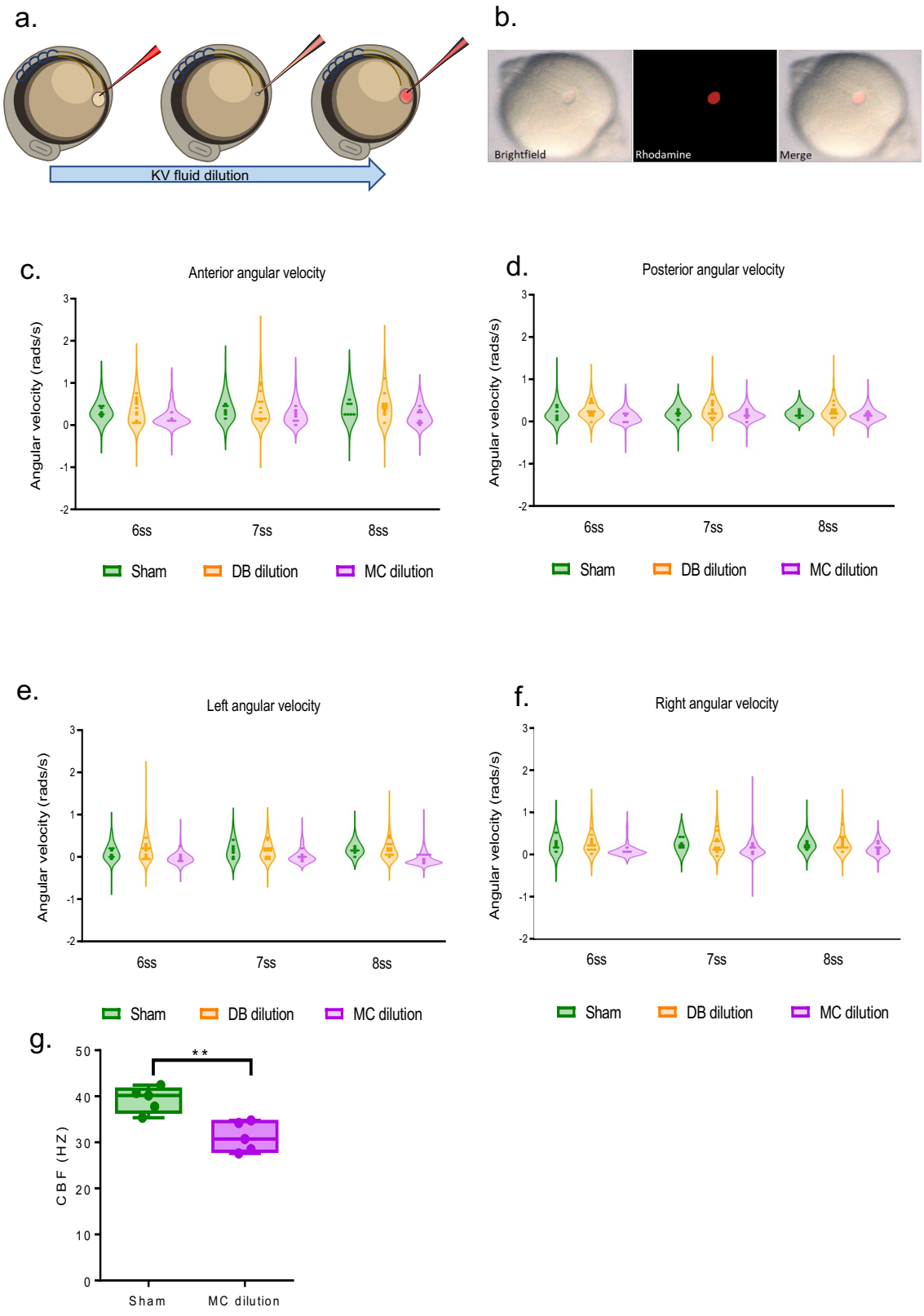

Figure 4 – **LRO fluid viscosity impacts on angular velocity and cilia beat frequency.** (a) Diagram of the dilution experiment: KV fluid is extracted by a needle previously loaded with fluorescent rhodamine-dextran diluted in Danieau buffer (DB) that, after mixing of the two liquids, are re-injected into the LRO (b) Example of a successfully micro-injected embryo labelled with fluorescent rhodamine-dextran. (c-f) Violin plots

showing the linear mixed model results for angular velocities (c) anterior, (d) posterior, (e) left and (f) right LRO quarters for Sham control embryos (in green), embryos with LRO fluid diluted with DB (in orange) and embryos diluted with MC (in purple). (g) CBF of the motile beating cilia in the 'Sham' control embryos versus embryos with LRO fluid diluted with MC. KV: Kupffer's vesicle; ss: somite stage; DB Danieau buffer; MC methylcellulose. A statistical linear mixed model was applied.

Moreover, these experiments demonstrated that following addition of MC but not DB alone, the resulting fluid flow affected *dand5* expression pattern, with more embryos displaying bilateral expression (7/12 embryos, 58%; Figure 5a, Fisher test, p-value < 0.001). Consistent results were obtained later in development for organ placement, with 56% of manipulated embryos showing misplacement of the heart position after MC treatment but not DB dilution alone (Figure 5b; Fisher test, p-value < 0.0001). Overall, these experiments provide the first direct evidence for flow mechanics determining LR development, in support of the mechanosensory mechanism. Indeed, if a signalling molecule contained in the LRO fluid was needed for *dand5* mRNA degradation, then the prediction would be that the DB dilution experiment resulted in many more embryos with *dand5* bilateral expression pattern than it did, as well as more heart misplacements.

Our observation that symmetry breaking is independent of the LRO fluid composition is consistent with the mechanosensory theory. Thus, as long as liquid volume and fluid dynamics are not changed for more than a few seconds, we showed that LR will be successfully established. Alternatively, if we attempt to interpret these results within a chemosensory mechanism, the dilution of a moving extracellular vesicle (EV) or molecule within could only occur without impacting LR if its secretion rate was sufficiently high to allow a fast turnover. This last hypothesis, however, is very unlikely and was refuted when we showed a limited response capacity to recover the asymmetric *dand5* expression, after a second extraction intervention (Figure S4) that was performed one hour later than the first extractions in the same embryos (Figure 1c).

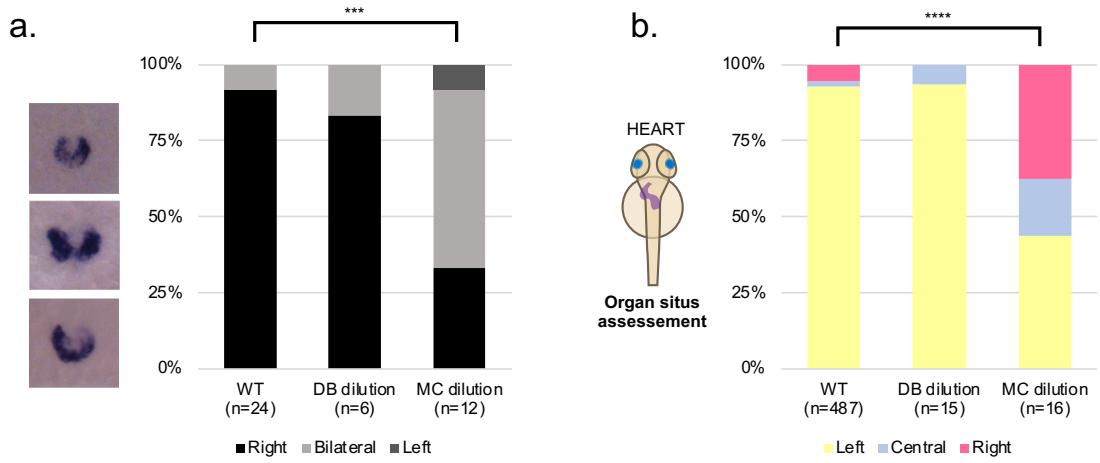

Figure 5 – **LRO fluid content does not affect left-right development.** (a) *dand5* mRNA expression pattern in wild-type control embryos, embryos with LRO fluid diluted with DB and embryos with LRO fluid diluted with MC. Embryos were fixed at 8 ss for *dand5* whole embryo *in situ* hybridization. (b) Heart position (left, central or right sided) was scored at 30 hpf in wild-type control embryos, embryos with LRO fluid diluted with DB and embryos with LRO fluid diluted with MC. ss: somite stage; DB Danieau buffer; MC methylcellulose; hpf: hours post fertilization.

A mathematical model of flow disruption, recovery, and signal integration predicts the experimental data

Our experimental data showed that one hour time-window, from 4 to 6 ss, is the most sensitive period to the fluid extraction challenge, exposing a relevant shorter developmental timing for early LR establishment. In addition, our data also demonstrated that anterior angular velocity is a crucial flow property. To better interpret the intervention results further and elucidate the probable importance of each somite stage in left-right patterning, we constructed a probabilistic mathematical model of how anterior angular velocity, integrated from 3 ss to 8 ss, produces a symmetry-breaking signal. Anterior angular velocity was modelled as a random variable, with mean and variance changing in time, and in response to intervention, based on mixed effects fitting to observed data and previously-reported observations of cilia density.

The unknown model parameters were the sensitivity weightings of the LRO to this angular velocity signal at each stage, with normal development occurring provided the integrated weighted signal exceeding a given threshold. Model parameters were then the six weightings relative to this threshold; parameters

were fitted to observed results by simulating 1000 virtual LROs for each intervention. Details of the model construction and fitting procedure are given in Supplementary information and Figures S12-S13.

The best fit for the full model showed good correspondence with observed experimental data (cf. Figure 1b and Figure 6a), in particular the highest defect rate close to 40% following intervention at 5 ss, and double intervention (5 ss+7 ss) producing a similar defect rate. This model assigned almost all of the stage weighting to 3 ss - 6 ss (Figure 6b). Taking account of the both stage weighting and anterior angular velocity, nearly 90% of the contribution to symmetry breaking occurred in the 4 ss - 6ss interval (Figure 6c).

To assess if models where only later stages were contributing to symmetry breaking could also explain the results, reduced models with each of 3 ss, 3-4 ss, 3-5 ss and 3-6 ss set to zero sensitivity were constructed in a similar manner to assess if observed results could in principle be matched without the contribution of these early stages (Figures 6d-o). The model omitting 3 ss contributions matched observed data similarly to the full model (cf. Figure 1b and Figure 6d). Omitting both 3 ss and 4 ss contributions led to qualitatively similar results (Figure 6g), slightly underpredicting the effect of 4 ss intervention and predicting 5 ss and 5 ss + 7 ss interventions would lead to a higher defect rate than observed. This model assigned almost all the contribution to the 5 ss stage (Figure 6i).

Omitting 3 ss - 5 ss contributions led to clearly incorrect predictions of the effect of 6 ss intervention (Figure 6j) and omitting 3 ss - 6 ss contributions led to a model that was not able to make any match to observations (Figure 6m). Overall, these results emphasised the crucial contribution of the 5 ss and 6 ss stages, and possible contribution also of the 4 ss stage, to producing the results observed experimentally.

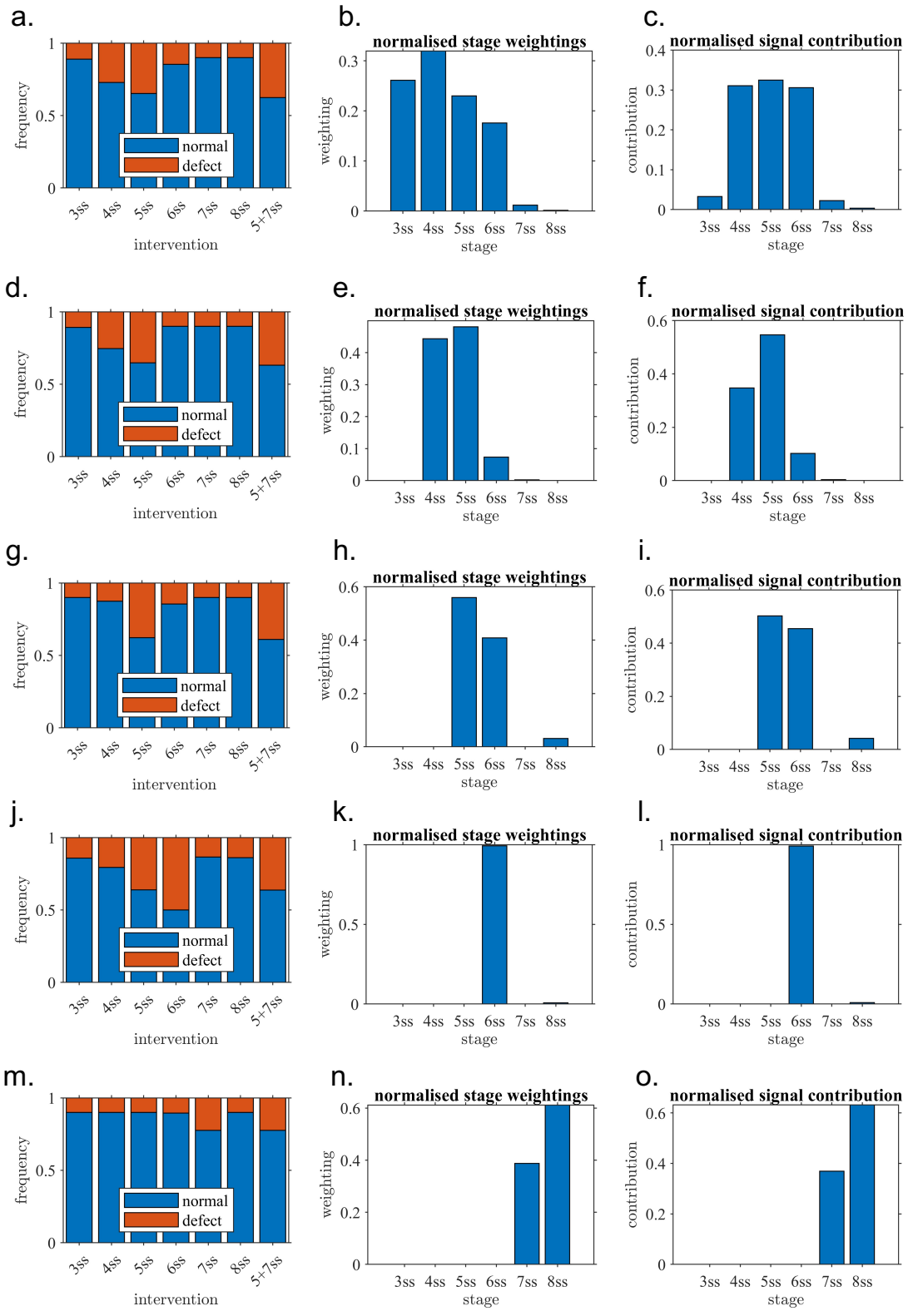

Figure 6 – **Mathematical modelling confirms the critical role of one-hour interval confirming the experimental observations.** (a) full model outputs, fitted to experimental observations in Figure 1b; (b) stage weightings (model parameters $W(t)$) for best fit model and (c) stage contributions, calculated by multiplying weightings by

average anterior angular velocity. (d-f) model with 3 ss weighting constrained to zero, (g-i) 3 ss - 4 ss weightings constrained to zero, (j-l) 3 ss - 5 ss weightings constrained to zero, (m-o) 3 ss - 6 ss weightings constrained to zero. ss: somite stage.

Discussion

By challenging the zebrafish left-right organizer (LRO) with a new form of manipulation we tested the time limits for the generation of asymmetric signals coming from the LRO, a transient embryonic organ. With this information we established a temporal map for the occurrence of symmetry breaking, highlighting the most sensitive developmental stages and its flow dynamics. We narrowed the LR time-window to 1 hour (Figure 1b). After manipulation at 5 ss, we studied flow recovery dynamics from 6 to 8 ss, carefully analysing progression of fluid angular velocity components and flow directionality (Figures 2 and 3). While most embryos succeed to display a correct LR organ *situs* and do so by quickly restoring flow and compensating in anterior angular velocity, even with a significantly smaller LRO luminal area (Figure S2), others failed to do so. In these embryos with LR defects we found a general decreased anterior angular velocity, a smaller difference between anterior-posterior angular velocity and an abnormal flow directionality in anterior sections of the LRO. Therefore, we have identified the most sensitive properties of LRO flow and regions to be placed anteriorly.

Yuan et al (2015) showed that the intraciliary calcium signal intensity peaked on the left side of the LRO around 3 ss. This period coincides with the first defects we observed upon depletion of the LRO fluid content. Nevertheless, results and modelling showed that these younger embryos may have greater tolerance to challenges and higher chances of recovering the normal LRO flow parameters and subsequent correct LR pattern than those extracted at 5 ss.

The most susceptible timing to fluid manipulation challenge was 5 ss. Other studies showed that a process of LRO remodelling occurs between 4 and 6 ss resulting in a biased ciliary distribution to the anterior region (Wang et al 2011). It is also at this stage that we previously observed an increased number of motile cilia at the expense of immotile cilia, in robustness of the fluid flow and in establishment of characteristic patterns of fluid dynamics, such as the higher flow speed in the anterior dorsal pole (Tavares et al., 2017). Considering these results,

it would be tempting to suggest that the process of cell remodelling is a landmark after which the LRO becomes insensitive to challenges. If the challenge is made until 6 ss we demonstrated here that there is evidence for an active sensory mechanism that restores fluid and flow. This heightens the need of identifying the mechanism that senses fluid flow magnitude. Such sensory mechanism seems to be sensitive to flow properties, as viscosity, rather than to tension on the walls of the LRO lining cells. In the presence of a low Reynolds number, when viscosity dominates and inertia is negligible, a sensory system to be efficient must be very sensitive to lower flow magnitude as suggested in Shinohara et al. (2012). The most probable mechanosensory system in the zebrafish LRO involves Pkd1l1 and Pkd2 both present in the LRO cilia as shown by immunofluorescence (Roxo-Rosa and Lopes, 2020; Jacinto et al., 2021) and although it has not been possible to demonstrate that these proteins function together as a mechanosensory complex in zebrafish, there is evidence to be the case in the mouse node (Field et al., 2011). Moreover, patients with mutations in PKD1L1 or in PKD2 present laterality phenotypes such as *situs inversus*, heterotaxia and congenital heart disease (Bataille et al., 2011; Oka et al., 2014; Le Fevre et al., 2020).

According to flow modelling studies by Ferreira et al. (2017) it was estimated that a detection mechanism dependent on mechanosensory immotile cilia would need more than 44% of immotile cilia. Live quantifications of cilia motility along time, using 2-photon microscopy in Tavares et al. (2017) attest that in the first stages after the formation of the LRO, there are many more immotile cilia (around 94%) than motile, but then, a gradual loss of cilia immotility occurs during development (Tavares et al., 2017). The present study showed that in all embryos that developed correct LR ('Sham' and 'No defects' groups; Table S1) scored at 6 ss, very few immotile cilia were present (9 on average) in a total average of 43 cilia (n = 13 embryos), which is only 20,9% of the total LRO cilia. So, according to Ferreira et al. (2017), this fact brings to light that perhaps immotile cilia number is not a crucial factor after all. However, focusing the analysis on motile cilia number, our current findings are compatible with a previous fluid mechanics model for the LRO (Sampaio et al., 2014) where it was estimated that, at least 30 motile cilia are needed for a correct LR outcome.

A more recent hypothesis for the sensory system in the zebrafish embryo postulates that cilia themselves may sense their own movement (Ferreira et al., 2019). In fact, Yuan et al (2015) filmed intraciliary calcium oscillations (ICOs) in the zebrafish LRO motile cilia in action and showed that ICOs were abrogated in knockdowns of Pkd2 or of cilia motility genes. The motile cilia self-sensing model becomes appealing in view of the flow response to increased viscosity in the current study (Figures 4 and 5). Motile cilia pattern and power are known to differ at increasing viscosities (Gueron and Levit-Gurevich, 1998; Wilson et al., 2015; Kikuchi et al., 2017), which could potentially be measured by a ciliary membrane mechanosensor. In summary, we suggest that a ciliary mechanosensory system, such as Pkd1l1/ Pkd2 could be sensitive to flow magnitude. The fact that CBF is significantly lower in the methylcellulose injected embryos (Figure 4g) suggests that may be there is a minimum CBF threshold for the sensory system to generate efficient ICOs. Then, how such ICOs could lead to *dand5* mRNA degradation specifically on the left cells of the LRO is not resolved in zebrafish, but according to Yuan et al. (2015) there is an increase of left-sided ICOs in the early time points that seems to coincide with the crucial time-window we have now established. However, our data does not show a consistent difference in left versus right angular velocity and correct LR development, leading us to suggest that anterior flow is the relevant factor not left.

Research on LR establishment is moving forward regarding the role of calcium using the mouse model. A previous study by Delling et al. (2016) contradicted the idea that crown cells LRO cilia are good calcium-responsive mechanosensors. Conversely, recent work from Hamada's lab (Mizuno et al., 2020) demonstrated that LR asymmetric intraciliary calcium transients can be in fact detected at the node. Mizuno and colleagues further revealed that discrepancies between the two studies relate to the culture conditions used, which led calcium signals to be missed in the work by Delling et al. (2016). Moreover, recently, Minegishi et al. (2021) unveiled that in the mouse model, the 3′-UTR of *dand5* mRNA responds to the direction of fluid flow in a Pkd2-dependent manner via stimulating Bicc1 and Ccr4-Not. Together, these molecular players seem to mediate Dand5 mRNA degradation specifically on the left side of the mouse node. Our independent fluid

manipulations support a very sensitive mechanosensory system for the initiation of the LR pathway, but it remains to be demonstrated how and what exactly is sensed by the system, is it flow direction or flow magnitude? Our data highlights anterior flow magnitude as a major mechanical property in LR. Interventions that decreased flow magnitude or reduced its A/P difference were the ones that generated abnormal LR outcomes.

The time lag and complexity of the recovery process motivated the development of a mathematical model of flow and its developmental influence, and the effect of experimental interventions. Statistical modelling of normal and disrupted flow, and fitting of a 'weighted contribution' model to infer the relative importance of each somite stage in explaining the results, confirmed the critical importance of 5 ss and 6 ss in symmetry breaking, possible involvement of 4 ss also, and the limited role for flow during 7 ss and 8 ss. The process of constructing the model also emphasised that intervention has two effects: the transient gross reduction in flow associated with removal of the entire luminal fluid, but also a greater variance of flow following recovery – hence observed defects are as much a consequence of a proportion of embryos making a below average recovery, as the interruption itself.

References

Bataille, S., Demoulin, N., Devuyst, O., Audrézet, M. P., Dahan, K., Godin, M., Fonts, M., Pirson, Y., and Burtey, S. (2011). Association of PKD2 (Polycystin 2) mutations with left-right laterality defects. *American Journal of Kidney Diseases*. https://doi.org/10.1053/j.ajkd.2011.05.015

Brown, A. L., Johnson, B. E., and Goodman, M. B. (2008). Making patch-pipettes and sharp electrodes with a programmable puller. *Journal of Visualized Experiments*. https://doi.org/10.3791/939

Brown, K. T., and Flaming, D. G. (1974). Beveling of fine micropipette electrodes by a rapid precision method. *Science*. https://doi.org/10.1126/science.185.4152.693

Cartwright, J. H. E., Piro, N., Piro, O., and Tuval, I. (2007). Embryonic nodal flow and the dynamics of nodal vesicular parcels. *Journal of the Royal Society, Interface / the Royal Society*, *4*(12), 49–55. https://doi.org/10.1098/rsif.2006.0155

Essner, J. J., Amack, J. D., Nyholm, M. K., Harris, E. B., and Yost, H. J. (2005). Kupffer's vesicle is a ciliated organ of asymmetry in the zebrafish embryo that initiates left-right development of the brain, heart and gut. *Development (Cambridge, England)*, *132*(6), 1247–1260. https://doi.org/10.1242/dev.01663

Ferreira, R. R., Vilfan, A., Jülicher, F., Supatto, W., and Vermot, J. (2017). Physical limits of flow sensing in the left-right organizer. *ELife*, *6*, 1–27. https://doi.org/10.7554/eLife.25078

Field, S., Riley, K. L., Grimes, D. T., Hilton, H., Simon, M., Powles-Glover, N., Siggers, P., Bogani, D., Greenfield, A., and Norris, D. P. (2011). Pkd1l1 establishes left-right asymmetry and physically interacts with Pkd2. *Development*. https://doi.org/10.1242/dev.058149

Gueron, S., and Levit-Gurevich, K. (1998). Computation of the internal forces in cilia: application to ciliary motion, the effects of viscosity, and cilia interactions. *Biophysical Journal*, *74*(4), 1658–1676. https://doi.org/10.1016/S0006-3495(98)77879-8

Hojo, M., Takashima, S., Kobayashi, D., Sumeragi, A., Shimada, A., Tsukahara, T., Yokoi, H., Narita, T., Jindo, T., Kage, T., Kitagawa, T., Kimura, T., Sekimizu, K., Miyake, A., Setiamarga, D., Murakami, R., Tsuda, S., Ooki, S., Kakihara, K., … Takeda, H. (2007). Right-elevated expression of charon is regulated by fluid flow in medaka Kupffer's vesicle. *Development Growth and Differentiation*. https://doi.org/10.1111/j.1440-169X.2007.00937.x

Jacinto, R., Sampaio, P., Roxo-Rosa, M., Pestana, S., and Lopes, S. S. (2021). Pkd2 Affects Cilia Length and Impacts LR Flow Dynamics and Dand5. *Frontiers in Cell and Developmental Biology*, *9*, 624531. https://doi.org/10.3389/fcell.2021.624531

Kikuchi, K., Haga, T., Numayama-Tsuruta, K., Ueno, H., and Ishikawa, T. (2017). Effect of Fluid Viscosity on the Cilia-Generated Flow on a Mouse Tracheal Lumen. *Annals of Biomedical Engineering*, *45*(4), 1048–1057.

https://doi.org/10.1007/s10439-016-1743-y

Le Fevre, A., Baptista, J., Ellard, S., Overton, T., Oliver, A., Gradhand, E., and Scurr, I. (2020). Compound heterozygous Pkd1l1 variants in a family with two fetuses affected by heterotaxy and complex Chd. *European Journal of Medical Genetics*. https://doi.org/10.1016/j.ejmg.2019.04.014

McGrath, J., Somlo, S., Makova, S., Tian, X., and Brueckner, M. (2003). Two populations of node monocilia initiate left-right asymmetry in the mouse. *Cell*. https://doi.org/10.1016/S0092-8674(03)00511-7

Mizuno, K., Shiozawa, K., Katoh, T. A., Minegishi, K., Ide, T., Ikawa, Y., Nishimura, H., Takaoka, K., Itabashi, T., Iwane, A. H., Nakai, J., Shiratori, H., and Hamada, H. (2020). Role of Ca2+ transients at the node of the mouse embryo in breaking of left-right symmetry. *Science Advances*. https://doi.org/10.1126/sciadv.aba1195

Navis, A., Marjoram, L., and Bagnat, M. (2013). Cftr controls lumen expansion and function of Kupffer's vesicle in zebrafish. *Development (Cambridge, England)*, *140*(8), 1703–1712. https://doi.org/10.1242/dev.091819

Nonaka, S., Tanaka, Y., Okada, Y., Takeda, S., Harada, A., Kanai, Y., Kido, M., and Hirokawa, N. (1998). Randomization of Left–Right Asymmetry due to Loss of Nodal Cilia Generating Leftward Flow of Extraembryonic Fluid in Mice Lacking KIF3B Motor Protein. *Cell*, *95*(6), 829–837. https://doi.org/10.1016/S0092-8674(00)81705-5

Oka, M., Mochizuki, T., and Kobayashi, S. (2014). A novel mutation of the PKD2 gene in a Japanese patient with autosomal dominant polycystic kidney disease and complete situs inversus. *American Journal of Kidney Diseases : The Official Journal of the National Kidney Foundation*, *64*(4), 660. https://doi.org/10.1053/j.ajkd.2014.05.023

R Ferreira, R., Fukui, H., Chow, R., Vilfan, A., and Vermot, J. (2019). The cilium as a force sensor-myth versus reality. In *Journal of cell science*. https://doi.org/10.1242/jcs.213496

Roxo-Rosa, M., Jacinto, R., Sampaio, P., and Lopes, S. S. (2015). The zebrafish Kupffer's vesicle as a model system for the molecular mechanisms by which the lack of Polycystin-2 leads to stimulation of CFTR. *Biology Open*, *4*(11), 1356–1366. https://doi.org/10.1242/bio.014076

Roxo-Rosa, M., and Santos Lopes, S. (2020). The Zebrafish Kupffer's Vesicle: A Special Organ in a Model Organism to Study Human Diseases. In *Zebrafish in Biomedical Research*. IntechOpen. https://doi.org/10.5772/intechopen.88266

Sampaio, P., Ferreira, R. R., Guerrero, A., Pintado, P., Tavares, B., Amaro, J., Smith, A. a., Montenegro-Johnson, T., Smith, D. J., and Lopes, S. S. (2014). Left-right organizer flow dynamics: How much cilia activity reliably yields laterality? *Developmental Cell*, *29*(6), 716–728. https://doi.org/10.1016/j.devcel.2014.04.030

Schweickert, A., Weber, T., Beyer, T., Vick, P., Bogusch, S., Feistel, K., and Blum, M. (2007). Cilia-Driven Leftward Flow Determines Laterality in

Xenopus. *Current Biology*. https://doi.org/10.1016/j.cub.2006.10.067

Shinohara, K., Kawasumi, A., Takamatsu, A., Yoshiba, S., Botilde, Y., Motoyama, N., Reith, W., Durand, B., Shiratori, H., and Hamada, H. (2012). Two rotating cilia in the node cavity are sufficient to break left–right symmetry in the mouse embryo. *Nature Communications*, *3*, 622. https://doi.org/10.1038/ncomms1624

Smith, D., Montenegro-Johnson, T., and Lopes, S. (2014). Organized chaos in Kupffer's vesicle: How a heterogeneous structure achieves consistent left-right patterning. *Bioarchitecture*, *4*(3), 119–125. https://doi.org/10.4161/19490992.2014.956593

Supp, D. M., Brueckner, M., Kuehn, M. R., Witte, D. P., Lowe, L. A., McGrath, J., Corrales, J., and Potter, S. S. (1999). Targeted deletion of the ATP binding domain of left-right dynein confirms its role in specifying development of left-right asymmetries. *Development (Cambridge, England)*, *126*(23), 5495–5504. http://www.ncbi.nlm.nih.gov/pubmed/10556073

Sutter Instrument, P-97 Pipette Cookbook. *Sutter Instrument*; 2008. http://www.sutter.com/contact/faqs/pipette_cookbook.pdf.

Takao, D., Nemoto, T., Abe, T., Kiyonari, H., Kajiura-Kobayashi, H., Shiratori, H., and Nonaka, S. (2013). Asymmetric distribution of dynamic calcium signals in the node of mouse embryo during left-right axis formation. *Developmental Biology*. https://doi.org/10.1016/j.ydbio.2013.01.018

Tanaka, Y., Okada, Y., and Hirokawa, N. (2005). FGF-induced vesicular release of Sonic hedgehog and retinoic acid in leftward nodal flow is critical for left-right determination. *Nature*, *435*(7039), 172–177. http://dx.doi.org/10.1038/nature03494

Wilson, K. S., Gonzalez, O., Dutcher, S. K., and Bayly, P. V. (2015). Dynein-deficient flagella respond to increased viscosity with contrasting changes in power and recovery strokes. *Cytoskeleton (Hoboken, N.J.)*, *72*(9), 477–490. https://doi.org/10.1002/cm.21252

Yuan, S., Zhao, L., Brueckner, M., and Sun, Z. (2015). Intraciliary Calcium Oscillations Initiate Vertebrate Left-Right Asymmetry. *Current Biology*, 1–12. https://doi.org/10.1016/j.cub.2014.12.051

Acknowledgments:

This work was mainly supported by the Fundação para a Ciência e Tecnologia (research grant – PTDC/BEX- BID/1411/2014).

PS was funded by a PhD fellowship FCT: SFRH/BD/111611/2015.

SP was funded by a PhD fellowship FCT: SFRH/BD/130272/2017

IAT was funded by FCT Investigator IF/00082/2013, EU FP7-PEOPLE-2013-CIG (Nº 818743) and by the Fundação Calouste Gulbenkian (FCG).

AG thanks to CZI Expanding Global Access to Bioimaging and to PAPIIT (IN211821) for funding support.

DJS acknowledges support from the Engineering and Physical Sciences Research Council UK via a Healthcare Technologies Challenge Award (EP/N021096/1) and a Turing Fellowship (EP/N510129/1).

SL was funded by FCT Investigator IF/00951/2012, by NOVA Medical School and by FCT CEEC-IND 2018.

Zebrafish were reared and maintained in the NMS Fish Facility, with the support from the research consortia Congento funded by LISBOA-01-0145-FEDER-022170, microscopy was performed at the IGC Advanced Imaging Facility which is supported by PPBI-POCI-01-0145-FEDER-022122; all co-financed by Lisboa Regional Operational Program (Lisboa2020), under the Portugal 2020 Partnership Agreement, through the European Regional Development Fund (ERDF) and Fundação para a Ciência e Tecnologia under the project.

The project LysoCil funded by the European Union Horizon 2020 research and innovation under grant agreement No 811087 supported SL, PS and SP travelling to the FASEB cilia meeting in the USA in 2019, where this work was presented and discussed with peers.

Author contributions:

Conceptualization: SSL, IT, PS, DS

Methodology: PS, SP, IT, DS

Investigation: SSL, PS, DS,

Visualization: SSL, DS

Funding acquisition: SSL

Project administration: SSL

Supervision: SSL, IT, AG, DS

Writing – original draft: PS, SSL

Writing – review & editing: SSL, IT, SP, PS, DS, AG

Competing interests: Authors declare that they have no competing interests.

Data and materials availability:

All data are available in the main text or the supplementary materials.

Science
AAAS

Supplementary Materials for

Fluid manipulations uncover mechanosensation for zebrafish left-right establishment during one-hour time interval

Pedro Sampaio, Sara Pestana, Adán Guerrero, Ivo Telley, David J. Smith, Susana S. Lopes.

Correspondence to: susana.lopes@nms.unl.pt and D.J.Smith@bham.ac.uk

This PDF file includes:

Materials and Methods

Supplementary Text

Figs. S1 to S13

Table S1-S3

Captions for Movie S1

Other Supplementary Materials for this manuscript include the following:

Movie S1

Data scripts S1 to S4

Materials and Methods

Fish husbandry and strains

Zebrafish were maintained at 25°C or 30°C and staged as described elsewhere (Kimmel et al., 1995) according to the number of somites. The following zebrafish lines were used for this work: AB and Tg(sox17:GFP)s870 (Chung and Stainier, 2008). Procedures with zebrafish were approved by the Portuguese DGAV (Direção Geral de Alimentação e Veterinária).

LRO manipulation setup for liquid extraction

LRO manipulations of fluid extraction were performed from 3 to 12 somite stages (ss). Zebrafish embryos were individually chosen at the developmental time correspondent to each somite-stage. Furthermore, only embryos that recovered LRO fluid were used throughout the study. Individually embryos were hold from the anterior dorsal side of the body using a holding pipette while a second pipette was used to penetrate the LRO from the posterior dorsal side. After extracting the LRO liquid the microinjection pipette was withdrawn, and embryos were incubated and let to develop. Collectively 173 embryos were manipulated along the different stages. Embryos were let to develop at 28°C and were later characterized according to *dand5* expression pattern or to organ laterality.

The micromanipulation system, as illustrated in Figure 1, was composed of an inverted microscope (Andor Revolution WD, Oxford Instruments; or Nikon Eclipse Ti-U) with a 10x Plan DL air objective, a 60x Plan Apo VC water immersion and a 100x Plan Fluor oil immersion objective (Nikon), a set of two motorized axis manipulators (MPC-385-2, Sutter Instruments) placed on both sides of a culture dish for moving pipettes to the desired positions, a CMOS camera (Monochrome UI3370CP-M-GL, Imaging Development Systems GmbH; or high speed FASTCAM MC2 camera, Photron Europe, Limited) to capture images in the microscope field of view, and a set of two CellTram's (CellTram Vario, FemtoJet, Eppendorf). Each respective microinjector are connected to a holding micropipette for immobilizing the zebrafish embryo, and injection micropipette that allows fluid manipulation from or to the Kupffer's vesicle (KV).

All the setup components were constructed over an optical table with vibration isolation (ThorLabs) to minimize the effects of any residual vibrations or disturbances introduced during the embryo manipulation procedure.

Immobilizing embryos

The creation of a chamber for easy handling of the injection micropipettes while keeping the specimen in an aqueous solution was crucial for the success of this procedure. Using silicone grease (Dow Corning) a rectangular coating was outlined on a coverslip. Next, a sufficient amount of embryo medium E3 was carefully pipetted on the coverslip forming a liquid pond. This setup contained zebrafish embryos in an aqueous environment with very low physical impediment, allowing a high range of contact angle for micropipette manipulation to happen.

Pipette forging for micropipette extractions

During its developmental time period the LRO or KV will migrate from 70 to 120 μm below the tail mesodermal cell layer (Supatto et al., 2009). Consequently, vesicular fluid extraction and compound microinjection procedures require resistant sharp capillaries capable of piercing through the tail tissue dorsal to the KV. Micropipette tip size and shape of the taper are crucial factors determining if a micropipette will effectively impale the embryo tissue. Small tips and uniform tapers have the great advantage of causing less cell damage (Sutter Instrument, pipette cookbook, 2008). Likewise, a shorter tapered and very stiff micropipette is needed to penetrate very tough and rigid membranes.

Aluminosilicate glass capillaries are known to have an increased hardness and ability to form small tips compared with its borosilicate counterpart, allowing to form stiff longer tapers important for reaching the KV and avoiding unwanted tissue damage.

Taking this in consideration, microinjection pipettes (Aluminosilicate, inner diameter 0.68mm, outer diameter 1.00, length 10mm, without inner filament) were designed using a custom-made program in a horizontal filament puller (P-97 Micropipette Puller, Sutter Instrument). Reduced cone angle and slender taper can be achieved using a 2-loop puller program (Sutter Instrument, pipette cookbook, 2008).

The resulting pulled pipettes were often sealed or have a very narrow tip (<1 μm). Shaping the tip to the desirable size was important to avoid clogging of the pipette and

deliver a sharp cut when impaling the embryo tissue. Therefore, the tips of micropipettes were shaped to small apertures (<5 μm) under the microscope. Using the motorized manipulators, the tips were carefully cut-opened against a polished borosilicate capillary. This allows to have a balance between micropipette longevity and minimal tissue damage during embryo manipulation. For better results reducing the amount of mechanical stress caused by the needle injection, a micropipette beveller (BV-10, Sutter Instrument) was used to increase sharpness of the pipette tips (Brown and Flaming, 1974). This additional step was not always carried out due to the significant time increase in preparation of each micropipette.

Holding pipette

Since our organism of interest is immersed in an aqueous non-viscous solution, oscillations of the zebrafish embryo are a major concern during micromanipulation. Thus, special care should be taken to assure a rigid stable connection between the embryo tissue and the tip of the micropipette. To achieve this a holding pipette (typically positioned on the left side of the preparation), immobilized the specimen while an opposing injection micropipette (on the right side) was introduced into the embryo tail.

For forging holding pipettes, thin wall borosilicate capillaries (inner diameter 0.75mm, outer diameter 1.00mm, length 10mm, without inner filament) were used. Ideal holding pipettes have a flat straight break at the tip with large inner and outer diameter to provide better attachment and support to the zebrafish embryo. Fire-polishing was then performed to create a smooth surface to interface with the embryo tissue without damaging it, and produce an inner diameter (around 0.50mm) best suited to hold the embryo (example as described in Brown et al., 2008). A common Bunsen burner or a micro forge (MF-900, Narishige) were used to fire-polish the holding pipette.

Cilia number, length and anterior-posterior distribution in fixed samples

To ensure that low damage is caused during embryo manipulation we further quantified KV cilia number and length upon fluid extraction. After manipulation embryos were immediately fixed in PFA 4% and whole-mount immunostaining for acetylated α-tubulin was performed to label KV cilia as previously described (Lopes et al., 2010). Antibodies used for immunostaining were mouse anti-acetylated alpha-tubulin (1:400; Sigma) and and Alexa Fluor 488 (Invitrogen; 1:500). Cilia count and length measurements were

performed either manually or through semiautomated detection in IMARIS software program.

Evaluating motile / immotile cilia distribution by live imaging

Live embryos were injected at 1 cell stage with 50 pg of *arl13b-mCherry* and then later mounted in 1% (w/v) low-melting agarose at 5ss, covered in E3 medium. Live imaging was performed in a Zeiss LSM 710 confocal microscope with an Olympus 40x water immersion lens (NA 0.8) at room temperature. Stacks were then processed using Fiji for identification of motile and immotile cilia. Cilia identification was performed either manually or through semi-automated detection in IMARIS software program (Bitplane, UK). See supplementary text and figure below.

Live imaging of fluid flow in the zebrafish left-right organizer

For the LRO fluid extraction experiments, embryos were maintained between 28°C - 30°C until 5 ss, then mounted in a 2% (w/v) agarose mold and covered with E3 medium, and filmed at 25°C.

To evaluate the fluid flow and LRO inflation recovery dynamics, the LRO was followed along development, from 6 to 8 ss in a sample of embryos manipulated at 5 ss (n = 16). In parallel, embryos (n = 6) in which the LRO was punctured by a micropipette, without further liquid extraction, were used as controls ('Sham' group). Imaging was performed on a light microscope (Nikon Eclipse Ti-U inverted microscope), under a 60x/1.2 NA water immersion or 100×/1.30 NA oil immersion objective lens, by a FASTCAM-MC2 camera (Photron Europe Limited, UK) controlled with Photron FASTCAM Viewer software. Using the ImageJ plugin Measure Stack, the LRO was delineated, and its luminal area was measured in all focal planes. LRO particles were tracked using the ImageJ plugin MTrackJ as previously reported (Sampaio et al., 2014).

Evaluation of heart and gut laterality

Heart jogging was evaluated at 30 hours post fertilization (hpf) using a stereoscopic zoom microscope (SMZ745, Nikon Corporation). These embryos were then allowed to develop at 28ºC and at 53 hpf embryos were fixed and processed for *foxa3 in situ* hybridizations to assess gut laterality, or readily scored if a sox17:GFP transgenic line

was being used for the respective assay. We could then pair the heart *situs* with gut *situs* for each treatment and attribute an embryo *situs*.

Final organ *situs* score was attributed regarding the combined heart and liver lateralization status: *situs solitus* – normal organ patterning (left heart and liver), *situs inversus* - organs positioned opposite to normal positions (right heart and liver), and heterotaxia – comprising all the other laterality defects variants.

For the LRO fluid extraction assay a total of 1223 WT embryos and 173 manipulated embryos were characterized according to organ *situs*.

RNA in situ hybridization and immunofluorescence

Whole-mount *in situ* hybridization and immunostaining was carried out as before (Lopes et al., 2010). Digoxigenin RNA probes were synthesized from DNA templates of *dand5* (Hashimoto et al., 2004). *In situ* hybridization of *dand5* was performed from 8 to 10 somites-stage as described elsewhere (Thisse and Thisse, 2008).

Flow speed, angular velocity and particle directionality

The flow speed, angular velocities and velocity components were calculated by customized scripts in the program environment R (see below). The centre of the LRO was used as reference point of a polar coordinate system in which angles are expressed in radians. To study the flow dynamics near the LRO apical membrane, tracked points near the centre (corresponding to a circle with half of the LRO radius) were removed, as angular quantities are poorly defined along the axis of rotation, close to the centre of the LRO. Angular velocity represents the effective circular flow magnitude of a particle moving between two consecutive time frames. The centre of the KV was used as reference point of a polar coordinate system in which angles are expressed in radians. Instantaneous angular velocity (rad/sec) was calculated by dividing particle angle change by the time between consecutive image frames (0.2 seconds).

Particle directionality quantification at any given point was obtained by dividing the LRO in 30 degree sections and calculating the change of particle angle between two consecutive time frames, where the axis of the reference is the position of the particle in the first time point. The particle directionality values range from 0 to 2π.

Fluid dilution and viscosity manipulation in the zebrafish LRO

The KV fluid dilution assay was performed by aspirating the vesicular fluid into a micropipette previously filled with Danieau's solution 1x (58mM NaCl, 0.7mM KCl, 0.4mM MgSO4, 0.6 mM Ca(NO3)2, 5.0 mM HEPES pH 7.6) diluted in 10,000 MW rhodamine-dextran solution (1:4; Sigma-Aldrich). The mixed solution was injected again into the KV and only embryos with rhodamine-positive KV's were selected for the experiment. For viscosity manipulation, the micropipette was filled with Danieau's solution 1x containing 1.5% (w/v) of methylcellulose (M0555, Sigma). Aspirated KV fluid and methylcellulose were then injected again into the KV lumen until reaching the KV volume observed before the manipulation.

Statistical analysis

A Fisher's exact test performed with RStudio was used to compare frequency of left-right defects and *dand5* expression patterns between WT and manipulated embryos. To assess potential differences in KV area, cilia number, cilia length between WT and manipulated embryos Student's t-test was used. To assess area changes per somite Mann-Whitney U test was used. To assess cilia motility differences between anterior and posterior regions Fisher's exact test was used. Kolmogrov-Smirnov test was used from comparing particle trajectory distribution between two groups. Angular velocity data for tracks imaged in each of the suction and injection experiments were fitted to linear mixed effects models to characterise how angular velocity varies across LRO and over time, how these velocity field patterns are altered due to intervention, and how they are reflected by different embryo fates. Fixed effects were group (injection experiment: sham, buffer injection, methylcellulose; suction experiment: sham, no-defects, defects), somite stage, normalised posterior-anterior axis coordinate, normalised left-right axis coordinate, and interactions of group with somite stage, posterior-anterior and left-right coordinates. Random effects were included to account for heterogeneity between embryos in their response to intervention. The models were specified in Matlab (Mathworks) notation as,

Suction experiment:

$$AAV \sim 1 + Group*LR + Group*PA + Group*Time + (1 + Group \mid EmbryoID)$$

Injection experiment:

AAV ~ 1 + Intervention*LR + Intervention*PA + Intervention*Time + (1 + Intervention | Embryo ID)

Fitting was carried out with the command fitlme, with effects reported in the main text where p<0.05 and interpreted based on the sign and magnitude of the fitted coefficient. Full results are given below in Supplementary data.

Mathematical modelling

Mathematical models of anterior angular velocity, its disruption by suction intervention, and the signal integration process, were implemented as custom scripts in Matlab (R2021a, Mathworks, Inc, Natick MA).

Statistical models for anterior angular velocity

The key hypothesis of the model is that symmetry breaking is produced by anterior angular velocity AAV(t) at somite stage t integrated from 3 ss to 8 ss, weighted by the a priori unknown sensitivities W(t) at each stage.

Mixed effects models were fitted to anterior angular velocity data for 5 ss-intervention and sham intervention using the Matlab function nlmefit (nonlinear mixed-effects estimation).

AAV following intervention at 5 ss was modelled using the nonlinear function

$$AAV_{interv\_5ss}(t) = \varphi_1\left(\frac{1}{1+e^{-0.9(t-5-\varphi_2)}} - \frac{1}{1+e^{0.9\varphi_2}}\right) + \frac{\varphi_3}{1+e^{-8(t-5.5)}}$$

The coefficients 0.9 and 8 were chosen to provide a smooth increase from zero, and the parameters φ_j were determined by fitting. Mixed effects fitting produces estimates for the fixed effect (central tendency in the population) and the standard deviation of the random effect (quantifying variability in the population; to maintain parsimony only the final parameter φ_3 was modelled with a random effect. Estimates for the fixed effects were $\varphi_1 = 0.778 \pm 0.679$, $\varphi_2 = 0.969 \pm 2.562$ and $\varphi_3 = 0.126 \pm 0.249$. The random effect for φ_3 was estimated to be 0.169. While standard errors are relatively large, the purpose of the fitting process was not the parameter values per se, rather to obtain a representative model of the recovery process. The resulting model is shown in Supplementary Figure 12a .

AAV following sham intervention at 5ss was modelled using the linear function

$$AAV(t) = \varphi_1 + \varphi_2(t-5)$$

The intercept parameter φ_1 was modelled with a normally-distributed random effect. Estimates for the fixed effects were $\varphi_1 = 0.356 \pm 0.063$ and $\varphi_2 = 0.0362 \pm 0.0283$; the random effect for φ_1 was estimated to be 0.0378. The model is shown in Supplementary Figure 12b.

Experimental data were only available at 6 ss, 7 ss and 8 ss, following intervention at 5 ss. In the case of sham intervention, AAV at 3 ss - 5 ss was modelled based on observed AAV at 6 ss rescaled based on previously-observed data on motile cilia percentage, specifically 5.57% at 3 ss, 42.9% at 4 ss, 62.1% at 5 ss and 76.3% at 6 ss (so that $AAV(3) = (5.57/76.3)\ AAV(6)$ for example).

In the cases of intervention at 3 ss or 4 ss, the function $AAV_{interv\_5ss}(t)$ was shifted in time so that $AAV_{interv\_3ss}(t) = AAV_{interv\_5ss}(t+2)$, then for $3 \leq t \leq 5$ rescaled based on the motile cilia percentages given above.

The modelled AAV distributions for every case are given in Supplemental Figure 13.

Signal integration and symmetry breaking

Symmetry breaking signal S is modelled as a weighted sum at each somite stage,

$$S = \sum_{t=3}^{8} AAV(t)W(t)$$

Where the parameters $W(t)$ are the sensitivity weighting of each stage $t = 3, \ldots, 8$. The weightings are independent of the experimental situation and so are determined simultaneously across all experiment series.

A given embryo is assumed to break symmetry normally at a baseline rate of 50% in the absence of any signal at all, and at a rate of 90% if the signal exceeds a threshold (taken to be 1 in arbitrary units).

When sampling over 1000 embryos, the abnormality rate therefore lies between 50% and 90% depending on the distribution of signal S. This abnormality rate is used as the success probability for the binomial model used for model fitting.

Signal integration model fitting

There parameters W(t) are determined through maximum likelihood estimation combined with global search, treating each experiment series with a binomial model, with success probability determined from S as described above. The log-likelihood is then maximized through global optimization, by applying the MultiStart and GlobalSearch functions (Matlab Global Optimization Toolbox). A uniform initial guess $W(3) = W(4) = \cdots = W(8) = 1$ is supplied to MultiStart, which executes 100000 local solver runs starting in the set $[0,5]^6$. The output of MultiStart is then supplied to GlobalSearch as an initial guess, and the optimal value of the two solvers is taken as the best fit.

Restricted models

To assess whether alternative fits weighted to later somite stages could explain the data as well as the best fit to the full model, four restricted models were also assessed. These models enforced in turn $W(3) = 0$, $W(3) = W(4) = 0$, $W(3) = W(4) = W(5) = 0$ and $W(3) = W(4) = W(5) = W(6) = 0$.

Supplementary text

LRO fluid manipulation does not affect left-right placement of the internal organs

Our microinjection system aimed to enable smooth fluid manipulation of the LRO with minimal cell damage. To ensure that the micromanipulation procedure did not produce developmental side-effects on the embryos leading to left-right defects, several control tests were performed.

The embryo holding step is based on immobilization of the embryo by a pipette positioned on its left side in order to allow the injection micropipette to be introduced from the right side through the dorsal tissue into the KV. Of the several positions tested immobilization by the zone dorsal to the developing head of the embryo was the most effective. Unlike the yolk, the back of the head offered a resistant tissue with a shape that easily adapted to the diameter of the holding pipette. At the same time this setup allowed the KV to be aligned with the microinjection needle field of action. In 20 embryos tested none died or developed laterality defects afterwards.

The next objective was to ensure that the microinjection needle was introduced without causing damage to the KV wall, which could compromise the normal LR signalling. Therefore in 10 embryos tested, the needle was inserted inside the KV and then removed. None of the embryos presented laterality defects in the heart or gut after two days and no mortality was registered up to 6 days of development.

During the developmental time period of 3ss – 14ss, the diameter of the Kupffer's vesicle increased varying from a minimum of 28 to 72 μm (an estimated volume of 8 to 174 pL, as described by Ferreira et al. 2017 and Tavares et al, 2017). So, upon the manipulation of liquid into or out of the LRO it was predicted that there would be momentary disturbances in volume and fluid dynamics. Therefore, we checked whether fast variations in KV volume and fluid dynamics during the handling period would cause LR defects per se. The microinjection needle was introduced in 10 different embryos and all the liquid from the KV was extracted into the micropipette and restored after 5 seconds. In our experience a change of a couple fine rotatory steps on the microinjector was sufficient for picolitre volume manipulations in the KV. Under the microscope we could observe the ventral and dorsal wall of the KV collapsing into each other after fluid extraction and being reshaped back to its position after re-introduction of the fluid. Similarly, all embryos tested had no LR defects, for stages comprised from 3ss to 12ss.

LRO fluid extraction does not affect total cilia number or cilia anterior-posterior distribution

To ensure that low damage is caused during embryo manipulation we further quantified KV cilia number and length upon fluid extraction. After manipulation embryos were immediately fixed in PFA 4% and whole-mount immunostaining for acetylated α-tubulin was performed to label KV cilia as previously described (Lopes et al., 2010). Our results showed that embryos manipulated at 5 ss (n = 8) had a similar number, length and anterior-posterior (AP) ratio of KV cilia distribution compared to a non-manipulated control group (n = 8, Supplementary Figure 1). In conclusion, we have generated a versatile and robust micromanipulation system that allows extraction of liquid from the KV since the first steps of the organizer development (3 ss onwards).

Motile cilia beat frequency and motile /immotile cilia spatial distribution are unchanged in manipulated embryos with normal LR development

The LRO of zebrafish has motile and immotile cilia, (Tavares et al. 2017) (Supplementary Figure 2a). To check if extraction experiments interfered with cilia motility, we analysed cilia motility distribution and cilia beat frequency (CBF) of motile cilia, by high-speed video microscopy. When analysing CBF of motile cilia at 6 ss, Sham controls had an average of 38.93 Hz (n = 56 cilia; 6 embryos) and fluid extracted embryos had 37.85 Hz (n = 60 cilia; 6 embryos); meaning that no evidence of difference was found (Supplementary Figure 2b), even when we focused the analysis on anterior motile cilia (Sham controls had an average of 39.09 Hz; n = 27 cilia and manipulated embryos had an average of 38.46 Hz, n = 21 cilia).

To determine if after extraction at 5 ss there were significant anterior-posterior cilia distribution differences between 'Sham' and manipulated experimental groups the spatial distribution of cilia types were compared by live imaging (Supplementary Figure 2c) as well as the ratio of motile to immotile cilia (Supplementary Figure 2d). Using a fluorescent reporter for cilia (Arl13b-GFP), we determined these readouts at 6 ss after embryo manipulation at 5 ss (Supplementary Movie 1). Consistent with previous studies (Compagnon et al., 2014; Tavares et al., 2017), cilia from control 'Sham' embryos at 6 ss (n = 7) were predominantly motile (82 ± 4 SEM %) and localized preferentially to the anterior half of the LRO (Fisher test, p-value < 0.05, Supplementary Figure 2c). The total number of motile cilia for each analysed 'Sham' embryo ranged from 21 to 50 cilia, revealing some intrinsic embryo variability even among the control group as reported before (Sampaio et al., 2014). Similarly, in the manipulated group (n = 6 embryos), cilia were also motile (78 ± 10 %) and distributed more anteriorly (Fisher test p-value < 0.05, Supplementary Figure 2c). Therefore, no significant differences were found for the ratio of motile / immotile cilia between manipulated group compared to 'Sham' controls (Supplementary Figure 2d). As this analysis was done by live imaging, we could let the embryos grow and check their organ laterality. All sham and manipulated embryos in Supplementary Figure 2 had normal situs. These results led us to conclude that after extracting the LRO fluid, the flow recovery achieved by the manipulated group was accomplished due to enough motile cilia being present in the correct place. We found only 2 embryos which showed LR defects, one with very few motile cilia and the other without any striking defect (full data on Supplementary Table 1).

SUPPLEMENTARY FIGURES

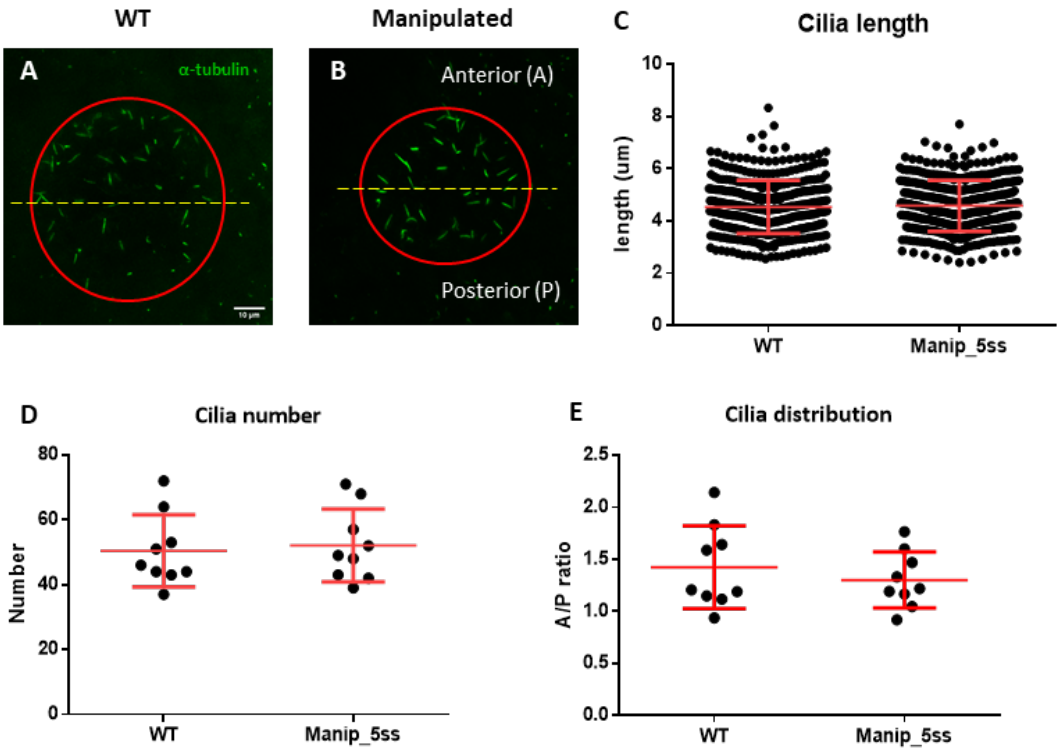

Supplementary Figure 1 – Manipulated embryos develop normal LRO cilia evaluated by immunofluorescence. ***Cilia number, length and anterior-posterior ratio of cilia distribution in WT and fluid extracted embryos – (a-b): Acetylated α-tubulin (in green) immunostaining examples showing LRO labelled cilia on WT and manipulated embryos. A number of 388 cilia in 8 WT embryos and 399 cilia in 8 manipulated embryos were measured in 3D (c). Mean cilia number (d) and A/P ratio (e) are displayed per embryo. Student's t-test was used to assess differences between groups.***

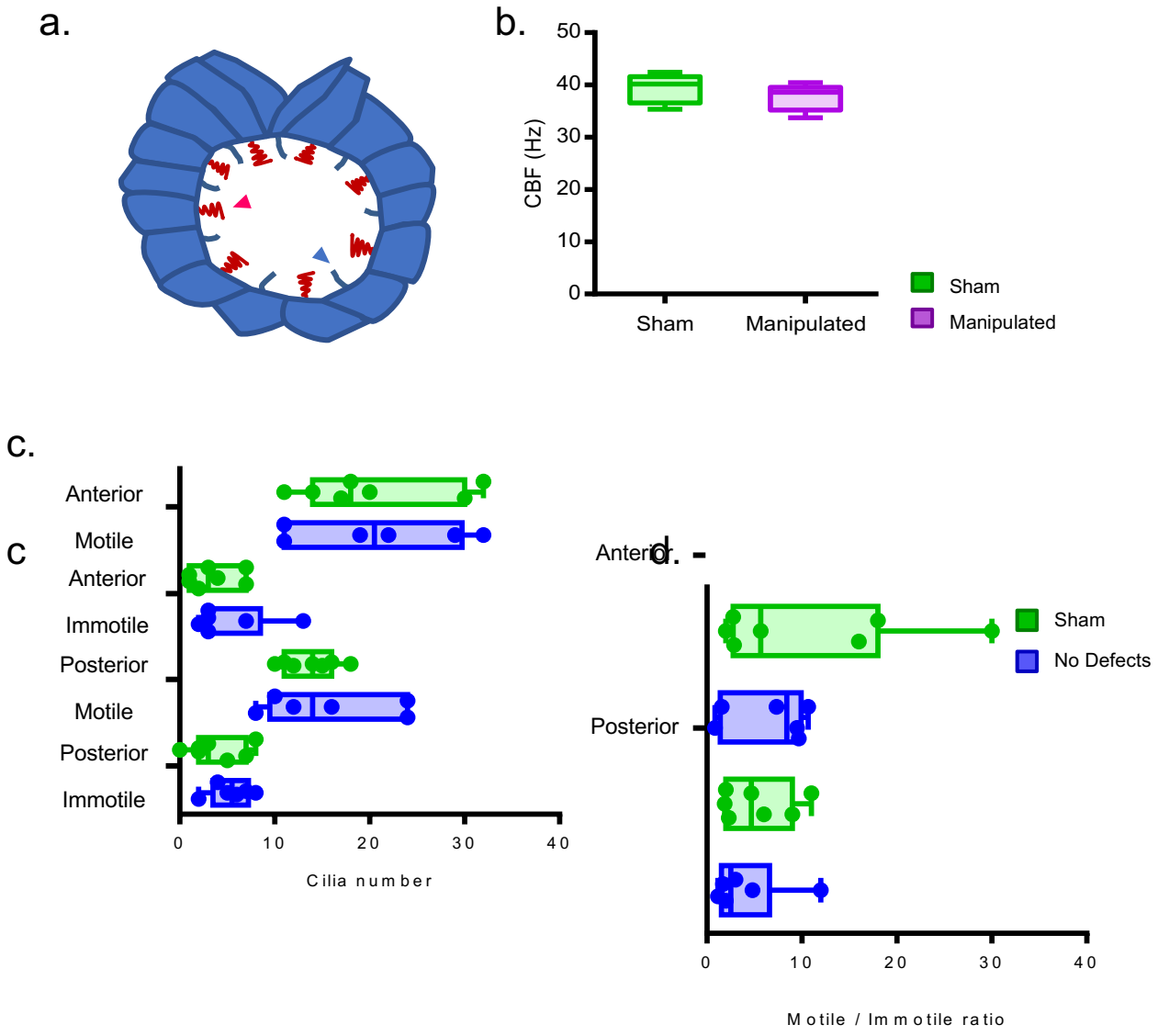

Supplementary Figure 2 – **Cilia Beat Frequency and motile/ immotile cilia ratio do not change in manipulated embryos evaluated by live imaging.** (a) Diagram highlighting motile and immotile cilia intercalated in the LRO cells. (b) CBF of the motile beating cilia that could be visualized by bright field live microscopy in the Sham control

embryos versus manipulated embryos (c) Total number of motile and immotile cilia located anteriorly and posteriorly between sham controls and embryos without LR defects. (d) Motile to immotile cilia ratio in the anterior and posterior LRO of Sham control embryos versus embryos that later developed without LR defects. Fisher's exact test was used to assess differences between treatments using pooled data from 6 embryos per treatment. Embryos were manipulated for LRO fluid extracted at 5 ss and were imaged at 6 ss. CBF: cilia beat frequency.

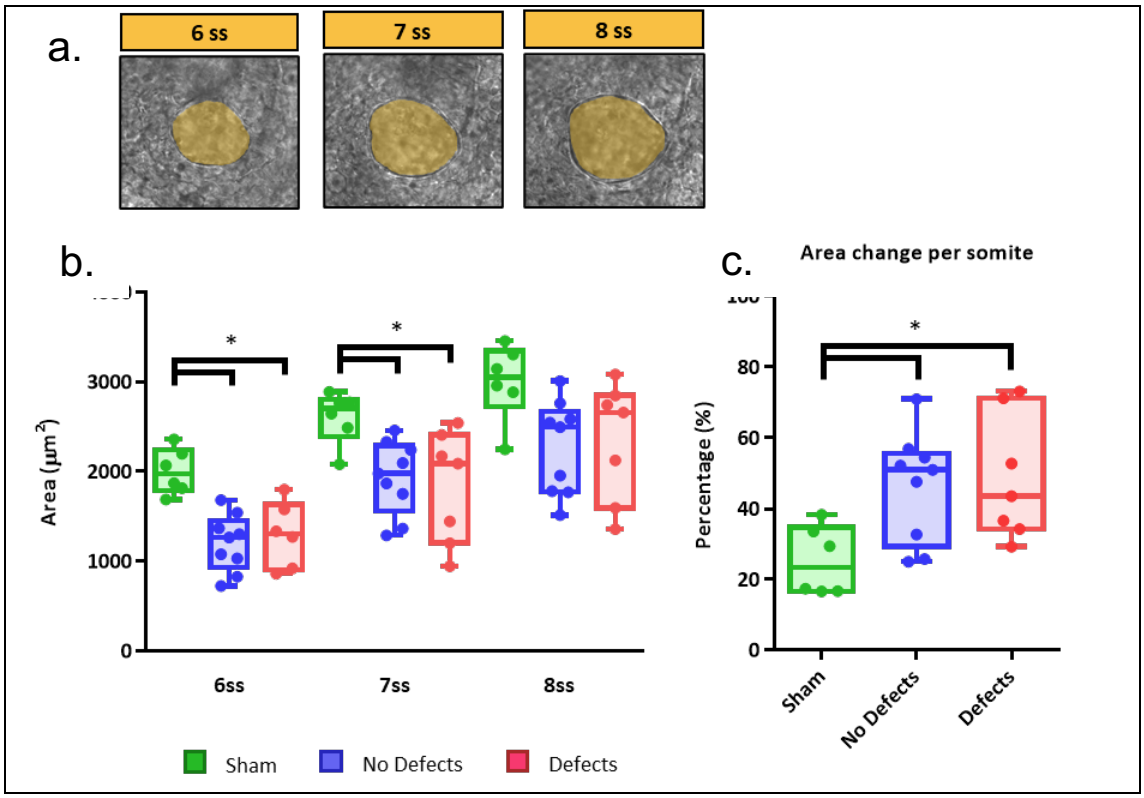

Supplementary Figure 3 – LRO areas from recovering embryos that develop left-right defects are not different from embryos that have a normal development. (a) LRO areas at 6-8 ss following extraction at 5 ss (b) Quantifications of LRO area of the three different groups ("Sham" control, "No Defects" and "Defects" group) in manipulated embryos during LRO lumen area recovery from 6 ss to 8 ss. (c) Area change per somite. Mann-Whitney U test p-value <0.05.

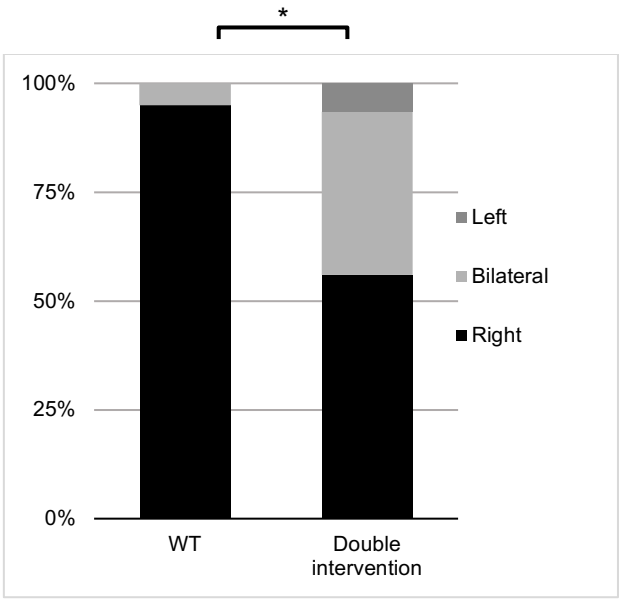

Supplemmentary Figure 4 - **A double extraction does not affect *dand5* expression pattern more than a single intervention.** After a double intervention for LRO fluid extraction, at 5 ss and at 7 ss *dand5* expression pattern was not significantly different from the single intervention result (Fisher test p-value > 0.05), although it was still significantly different from the WT (Fisher test p-value < 0.05).

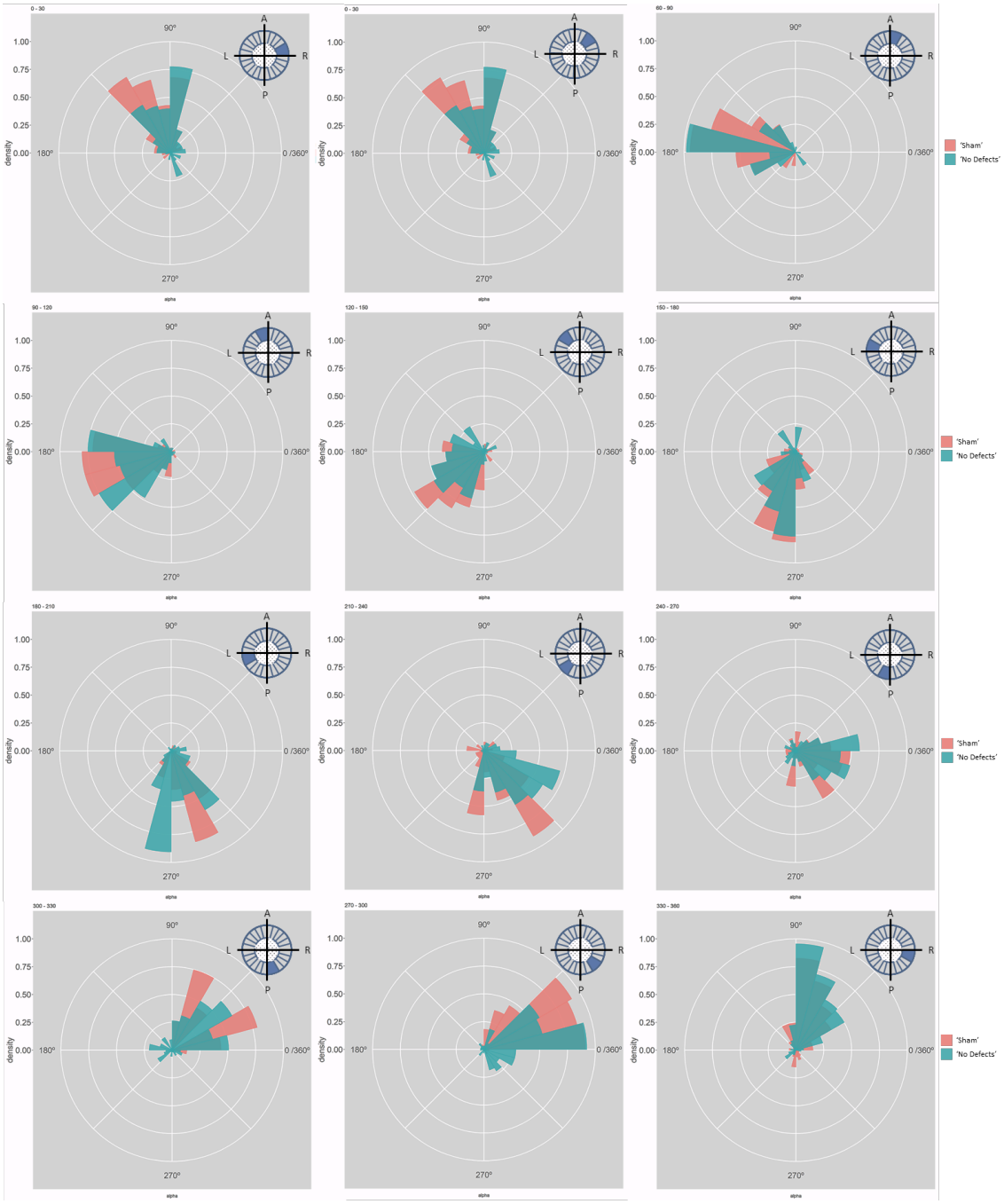
0 - 30
60 - 90
90 - 120
120 - 150
150 - 180
180 - 210
210 - 240
240 - 270
300 - 330
270 - 300
330 - 360
density
alpha
90°
180°
270°
0 /360°
A
L
R
P
1.00
0.75
0.50
0.25
0.00
'Sham'
'No Defects'

Supplementary Figure 5 – **Particle movement direction at different regions of the LRO for 'Sham' and 'No Defects' groups at 6 ss.** Each plot represents the pooled tracked trajectory of a moving particle at even given point in time. Trajectories were plotted from the outermost area of the LRO (radius > 0.5 from a maximum of 1). Kolmogorov-Smirnov test was used from comparing trajectory distribution between the two groups. KV: Kupffer's vesicle; ss: somite stage. LRO: left-right organizer.


0 - 30
30 - 60
60 - 90
90 - 120
120 - 150
150 - 180
180 - 210
210 - 240
240 - 270
270 - 300
300 - 330
330 - 360
density
alpha
90°
180°
0 /360°
270°
A
L
R
P
'Sham'
'Defects'

Supplementary Figure 6 – **Particle movement direction at different regions of the LRO for 'Sham' and 'No Defects' groups at 7 ss.** Each plot represents the pooled tracked trajectory of a moving particle at even given point in time. Trajectories were plotted from the outermost area of the KV's (radius > 0.5 from a maximum of 1). Kolmogrov-Smirnov test was used from comparing trajectory distribution between the two groups. KV: Kupffer's vesicle; ss: somite stage; LRO: left-right organizer.

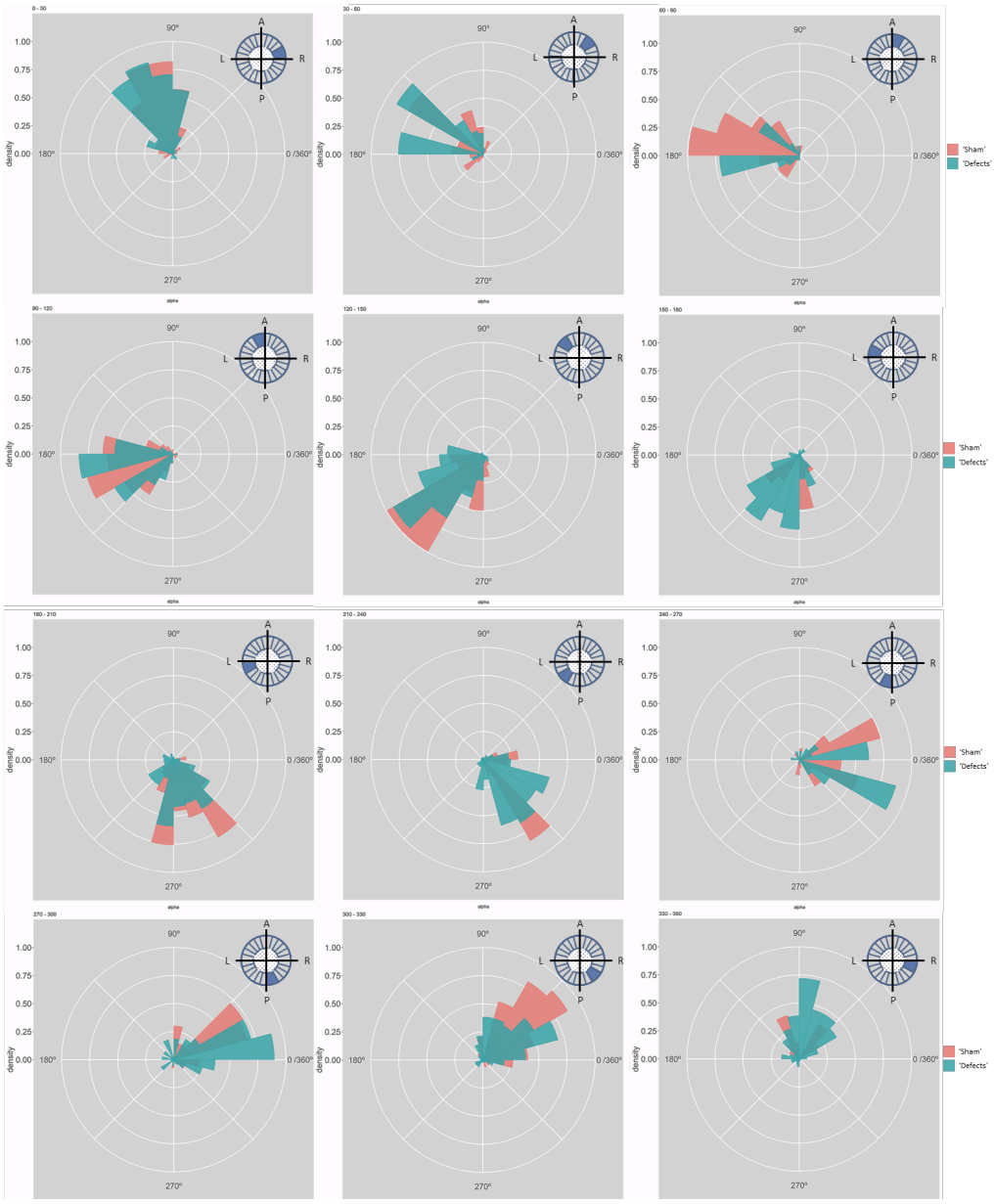
0 - 30
30 - 60
60 - 90
90 - 120
120 - 150
150 - 180
180 - 210
210 - 240
240 - 270
270 - 300
300 - 330
330 - 360
density
alpha
90°
180°
270°
0 /360°
A
L
R
P
1.00
0.75
0.50
0.25
0.00
'Sham'
'Defects'

Supplementary Figure 7 – **Particle movement direction at different regions of the LRO for 'Sham' and 'No Defects' groups at 8ss**. Each plot represents the pooled tracked trajectory of a moving particle at even given point in time. Trajectories were plotted from the outermost area of the KV's (radius > 0.5 from a maximum of 1). Kolmogorov-Smirnov test was used from comparing trajectory distribution between the two groups. KV: Kupffer's vesicle; ss: somite stage. LRO: left-right organizer.

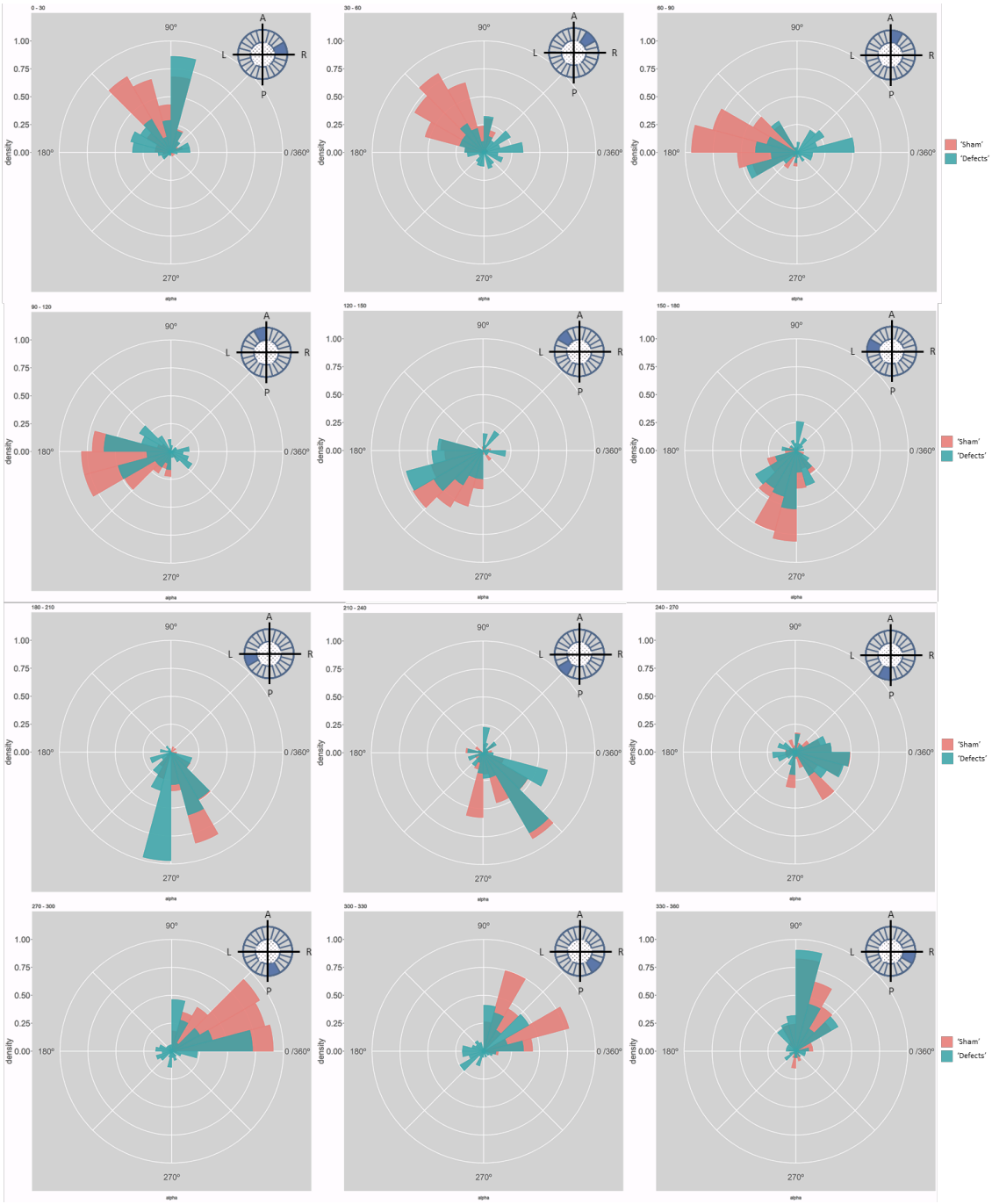
0 - 30
30 - 60
60 - 90
90 - 120
120 - 150
150 - 180
180 - 210
210 - 240
240 - 270
270 - 300
300 - 330
330 - 360
90°
180°
0 /360°
270°
A
L
R
P
density
alpha
1.00
0.75
0.50
0.25
0.00
'Sham'
'Defects'

Supplementary Figure 8 – **Particle movement direction at different regions of the KV for 'Sham' and 'Defects' groups at 6 ss.** Each plot represents the pooled tracked trajectory of a moving particle at even given point in time. Trajectories were plotted from the outermost area of the KV's (radius > 0.5 from a maximum of 1) Kolmogorov-Smirnov test was used from comparing trajectory distribution between the two groups. KV: Kupffer's vesicle; ss: somite stage. LRO: left-right organizer.

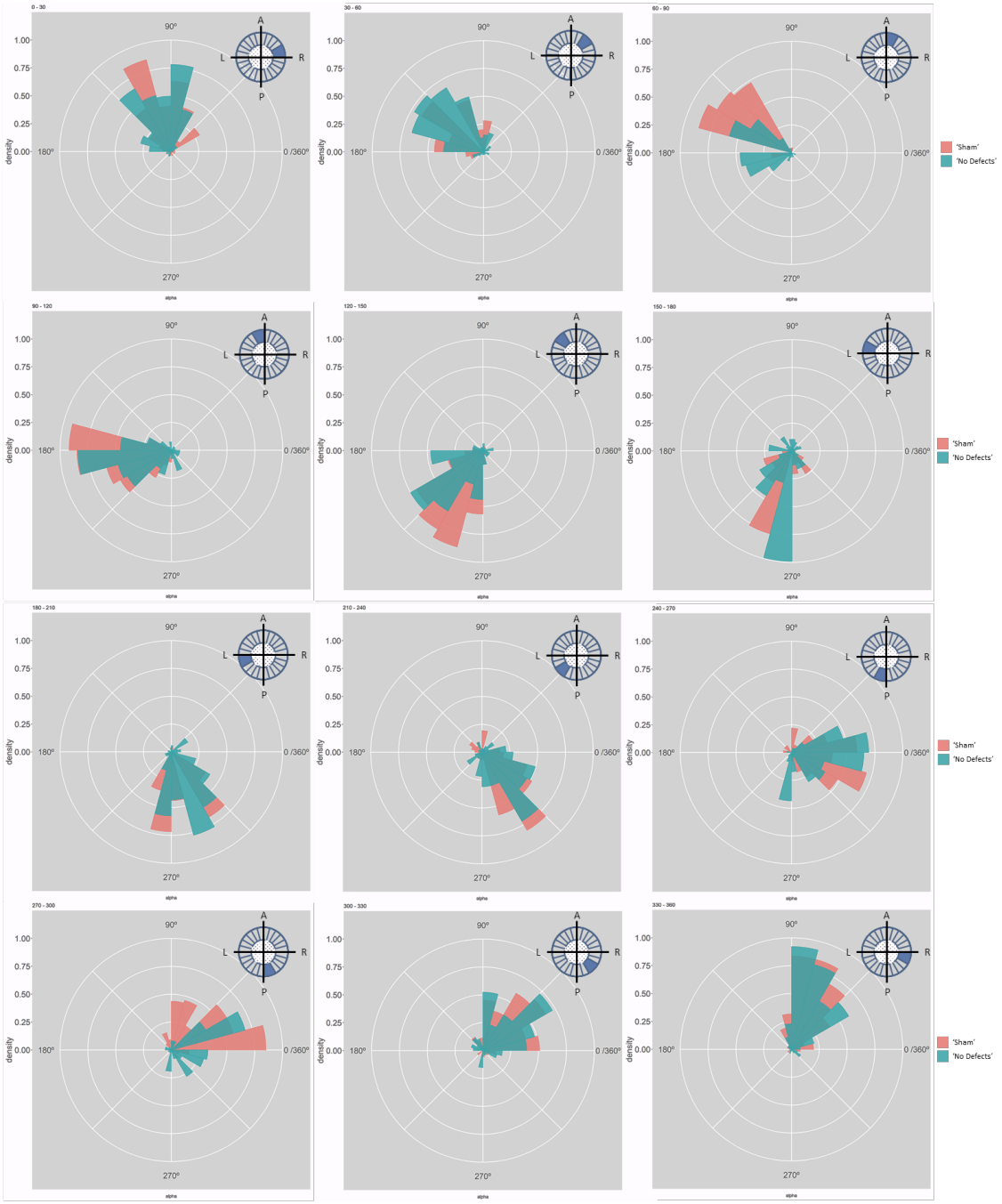
0 - 30
30 - 60
60 - 90
90 - 120
120 - 150
150 - 180
180 - 210
210 - 240
240 - 270
270 - 300
300 - 330
330 - 360
90°
180°
0 /360°
270°
A
L
R
P
density
alpha
1.00
0.75
0.50
0.25
0.00
'Sham'
'No Defects'

Supplementary Figure 9 – **Particle movement direction at different regions of the LRO for 'Sham' and 'Defects' groups at 7 ss.** Each plot represents the pooled tracked trajectory of a moving particle at even given point in time. Trajectories were plotted from the outermost area of the KV's (radius > 0.5 from a maximum of 1). Kolmogorov-Smirnov test was used from comparing trajectory distribution between the two groups. KV: Kupffer's vesicle; ss: somite stage. LRO: left-right organizer.

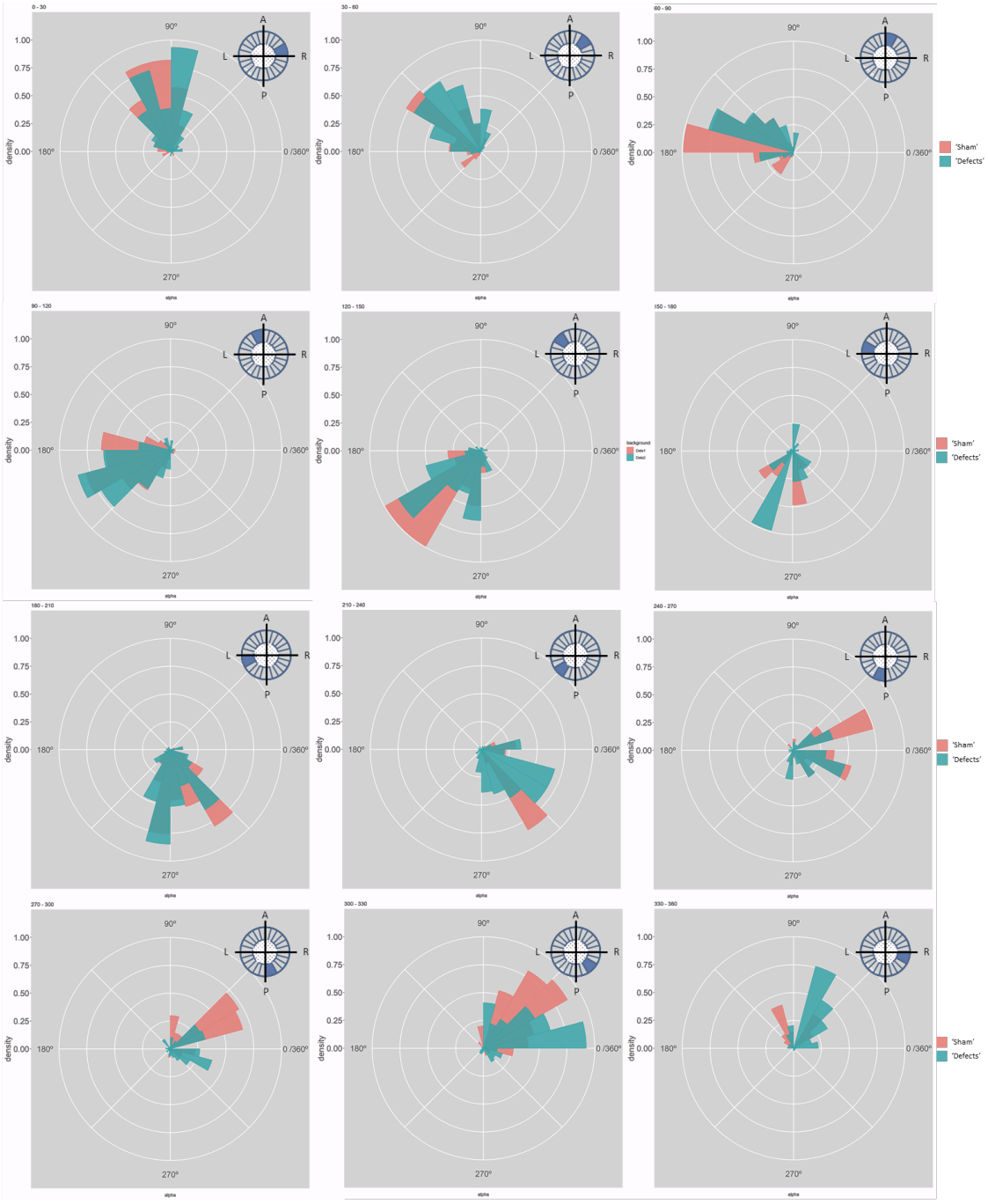
0 - 30
30 - 60
60 - 90
90 - 120
120 - 150
150 - 180
180 - 210
210 - 240
240 - 270
270 - 300
300 - 330
330 - 360
90°
180°
0 /360°
270°
A
L
R
P
density
alpha
1.00
0.75
0.50
0.25
0.00
'Sham'
'Defects'

Supplementary Figure 10– Particle movement direction at different regions of the LRO for 'Sham' and 'Defects' groups at 8 ss. Each plot represents the pooled tracked trajectory of a moving particle at even given point in time. Trajectories were plotted from the outermost area of the KV's (radius > 0.5 from a maximum of 1). Kolmogorov-Smirnov test was used from comparing trajectory distribution between the two groups. KV: Kupffer's vesicle; ss: somite stage. LRO: left-right organizer.

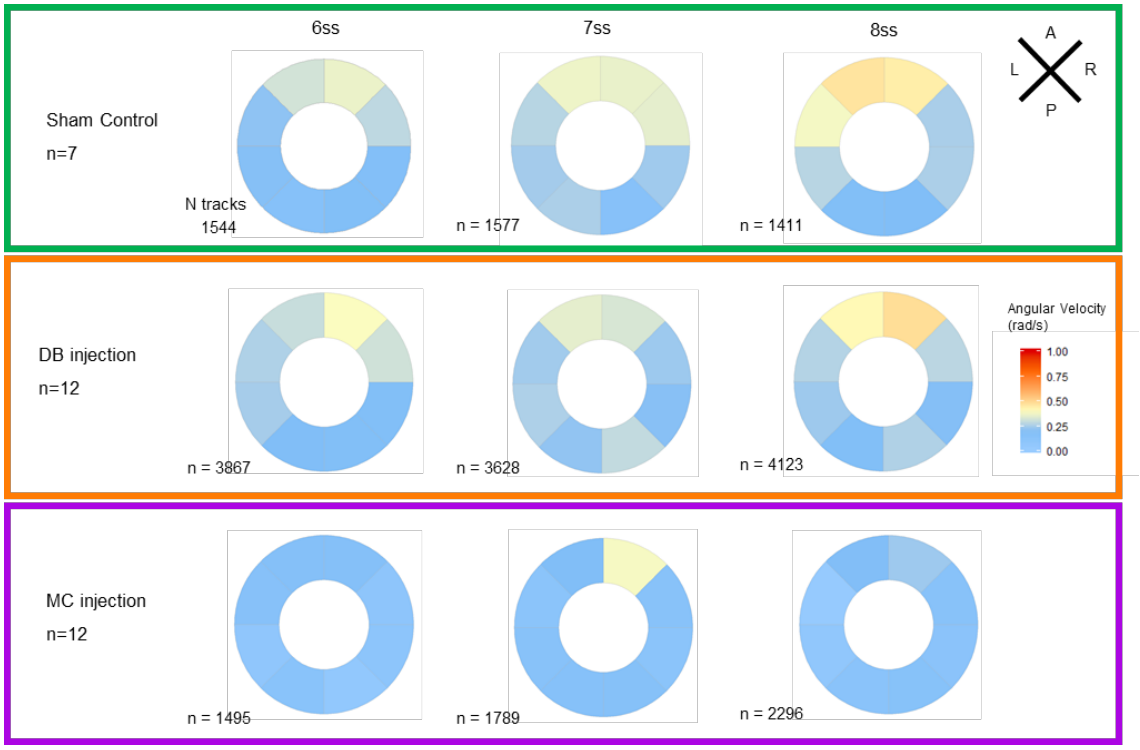

Supplemental Figure 11 -– LRO flow dynamics is only affected when fluid dilution alters fluid viscosity (a) Angular velocity polar plots for 6 ss, 7 ss and 8 ss for the three different groups (a) “Sham” control, (b) “DB dilution” group and (c) “MC dilution” group. Number of tracks refers to the number of particle trajectories identified for the quantifications and respective angular velocity plots. Colour code on polar plots refers to the median angular velocity for all pooled embryos.

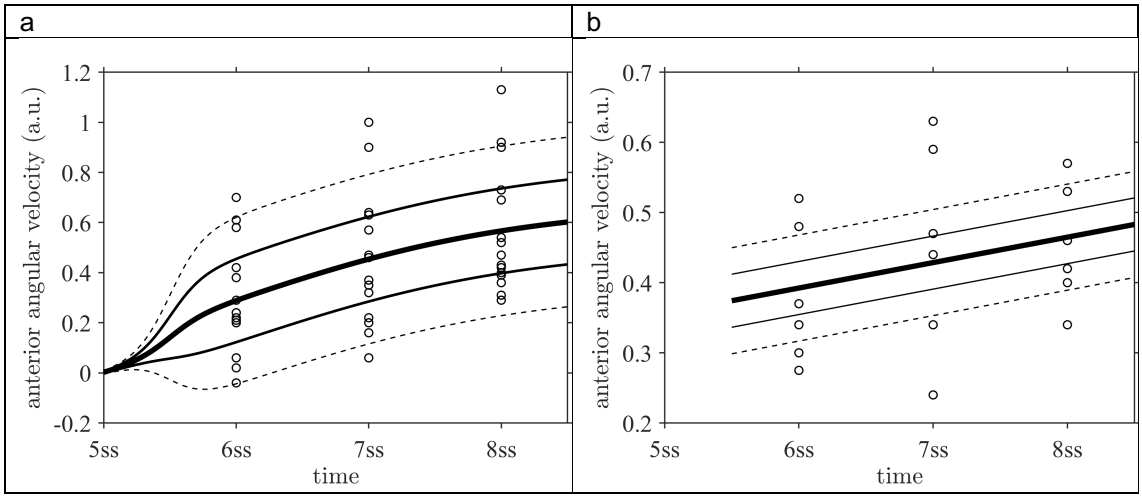

Supplementary Figure 12 – **Mixed effects model fits for the distributions of anterior angular velocity** to (a) data for sham intervention, (b) data for suction intervention at 5 ss. Central line is fixed effect, outer pairs of lines are +/- 1 and +/- 2 standard deviations in normally distribution random effects.

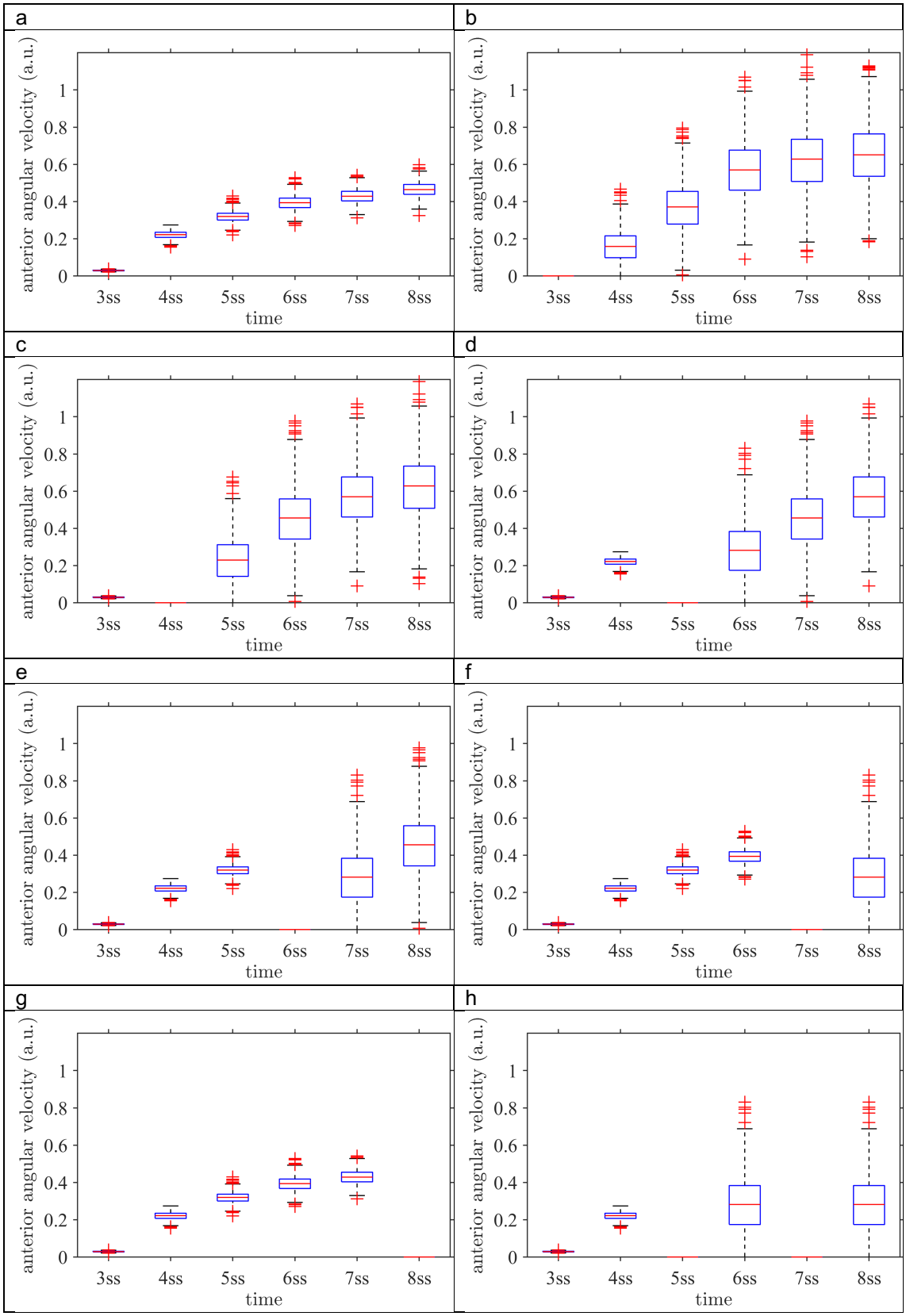

Supplementary Figure 13 - Anterior angular velocity distributions for all modelled experimental interventions. (a) sham, (b) 3 ss intervention, (c) 4 ss intervention, (d) 5 ss intervention, (e) 6 ss intervention, (f) 7 ss intervention, (g) 8 ss intervention, (h) both

5 ss and 7 ss intervention. These distributions are combined with stage weightings to fit the normal/defect percentages for each experiment series.

Table S1. Motile and immotile cilia distribution at 5 somite stage embryos.
Analyses of cilia motility per LRO anterior and posterior halves.

	Embryos	Anterior		Posterior		Total motile cilia	Total cilia
		Motile	Immotile	Motile	Immotile		
Sham	E1	32	2	18	2	50	54
	E2	20	7	15	8	35	50
	E3	11	4	10	5	21	30
	E4	18	1	11	0	29	30
	E5	17	3	12	2	29	34
	E6	30	1	16	7	46	54
	E7	14	7	14	3	28	38
No LR Defects	E1	22	3	16	8	38	49
	E2	11	7	10	6	21	34
	E3	19	2	12	4	31	37
	E4	21	2	24	5	45	52
	E5	32	3	24	2	56	61
	E6	11	13	8	7	19	39
LR Defects	E1	3	19	3	22	6	47
	E2	15	10	12	3	27	40

Table S2. Linear mixed-effects model fit: Results for fluid extraction experiment.

Fixed effects coefficient estimates are given. Model information: Number of observations: 15775; Fixed effects coefficients: 12; Random effects coefficients 69; Covariance parameters: 7. Model formula: AAV ~ 1 + Group*LR + Group*PA + Group*Time + (1 + Group | EmbryoID). Results relate to **Figures 2d-g;** *** indicates p<0.001; ** indicates p<0.01; * indicates p<0.05

Name	**Estimate**	**95% CI**	**p-value**
Intercept	0.25153 rad/s	0.20762 – 0.29544	3.8408e-29 ***
Group_2 (No defects)	-0.032775 rad/s	-0.12321 – 0.05766	0.47748
Group_3 (Defects)	-0.12728 rad/s	-0.18434 – -0.070215	1.2396e-05 ***
LR (left/right)	0.0042934 rad/s	-0.010776 – 0.019363	0.57655
PA (anterior/posterior)	0.16131 rad/s	0.14636 – 0.17626	6.285e-98 ***
Time	0.02145 rad/s/stage	0.012091 – 0.030809	7.0847e-06 ***
Group_2:LR	0.026653 rad/s	0.007577 – 0.04573	0.006176 **
Group_3:LR	-0.0026553 rad/s	-0.022753 – 0.017443	0.79567
Group_2:PA	0.033645 rad/s	0.012118 – 0.055171	0.0021912 **
Group_3:PA	-0.041406 rad/s	-0.06219 – -0.020622	9.461e-05 ***
Group_2:Time	0.026635 rad/s/stage	0.014317 – 0.038953	2.2637e-05 ***
Group_3:Time	0.013497 rad/s/stage	0.00056621 – 0.026427	0.040778 *

Table S3. Linear mixed-effects model fit: Results for Danieau buffer (DB) and methylcellulose (MC) dilution experiments. Fixed effects coefficient estimates are given. Model information: Number of observations: 16622; Fixed effects coefficients: 12; Random effects coefficients 90; Covariance parameters: 7. Model formula: AAV ~ 1 + Group*LR + Group*PA + Group*Time + (1 + Group | EmbryoID). Results relate to **Figures 5c-f.** Model formula: AAV ~ 1 + Intervention*LR + Intervention*PA + Intervention*Time + (1 + Intervention | EmbryoID). *** indicates p<0.001; ** indicates p<0.01; * indicates p<0.05

Name	Estimate	95% CI	p-value
Intercept	0.25148 rad/s	0.20891 – 0.29405	6.8705e-31 ***
Intervention_2 (DB)	0.070724 rad/s	-0.030824 – 0.17227	0.17223
Intervention_3 (MC)	-0.12344 rad/s	-0.19256 – -0.054311	0.00046626 ***
LR (left/right)	0.0042626 rad/s	-0.0081773 – 0.016702	0.50182
PA (anterior/posterior)	0.16135 rad/s	0.14901 – 0.17369	4.4137e-142 ***
Time	0.021413 rad/s/stage	0.013687 – 0.029139	5.6349e-08 ***
Intervention_2:LR	-0.012356 rad/s	-0.027636 – 0.002925	0.11301
Intervention_3:LR	0.026366 rad/s	0.0084783 – 0.044254	0.0038681 **
Intervention _2:PA	-0.02139 rad/s	-0.036997 – -0.0057835	0.0072282 **
Intervention _3:PA	-0.073208 rad/s	-0.092273 – -0.054142	5.4857e-14 ***
Intervention _2:Time	-0.012635 rad/s/stage	-0.022248 – -0.0030222	0.0099937 **
Intervention _3:Time	-0.0004407 rad/s/stage	-0.012174 – 0.011293	0.94131

Movie S1.

Evaluation of motile and immotile cilia distribution at 6 somite stage embryos. Injection of arl13b at 1 cell stage allows for visualization of motile versus immotile cilia. Anterior-posterior distribution was scored in 15 embryos that were later grouped as sham controls (normal situs), embryos with LR defects and without LR defects (Table S1).

Data scripts S1 to S4:

S1 Angular velocity

```
library(ggplot2)

require(plotrix)

require(grid)

require(circular)

require(lattice)

require(fields)
```

```
require(akima)
require(methods)
require(sp)



setOrigin <- function(xy, x0, y0, R, velFactor, pixelsToMicrons, fps = 1/0.2){
 x<- (xy[,4] - x0) / R
 y<- -(xy[,5] - y0) / R
 xreal<- (xy[,4] - x0)
 yreal<- -(xy[,5] - y0)
 id<-xy[,2]
 omega2 <- atan2(y,x)
  omega2.id <- which(omega2 < 0)
  omega2[omega2.id] <- 2*pi + omega2[omega2.id]
  omega <- atan2(x, y)
 r<- sqrt(x^2 + y^2)
   raioreal<-sqrt(xreal^2 + yreal^2)
 raioreal<-raioreal * pixelsToMicrons
 n<-length(x)
 a<-xy[,4][2:n] - xy[,4][1:(n-1)]
 b<-xy[,5][2:n] - xy[,5][1:(n-1)]
 alpha <-atan2(a, b)
 alpha.id <- which(alpha < 0)
 alpha[alpha.id] <- 2*pi + alpha[alpha.id]
 speed <- xy[,11]
 speed[is.na(speed)] <- 0
 rr<-sqrt(xreal^2 + yreal^2)


 p<- data.frame(x = x[1:(n-1)], y = y[1:(n-1)], id = id[1:(n-1)],
            omega = omega[1:(n-1)], r = r[1:(n-1)],
            alpha, speed = speed[2:(n)] * velFactor,rr = rr[1:(n-1)],omega2 = omega2[1:(n-1)])
  for (i in 1:length(p$id)) {
 dr<-rr[2:n] - rr[1:(n-1)]
 }
```

```
 p$vr<-dr*velFactor
 p$vr[p$speed==0] <- 0
for (j in 1:length(p$id)) {
  domega<-omega2[2:n] - omega2[1:(n-1)]
 }
 p$domega <- domega
 vt<- rr[2:n]*sin(domega)
 p$vt<-vt*velFactor
 p$vt[p$speed==0] <- 0
 dang<-sin(domega)
 realangvel<-asin(dang)
 p$realangvel<-realangvel*fps
 p$realangvel[p$speed==0]<- 0
 return(p)
}
```

S2 Particle directionality

```
direction.graph <- function(Data, Data2, Name2, minR = 0.5, omegares = 30, na.rm = TRUE){

 Data <- subset(Data, r > minR)
 omega1<-Data$omega
 alpha1<-Data$alpha
 angvel1<-Data$angvel
 r1<-Data$r
 omega1<-omega1 - pi/2
 alpha1<-alpha1 - pi/2
 omega1.id <- which(omega1 < 0)
 omega1[omega1.id] <- 2 * pi + omega1[omega1.id]
 omega1<-(omega1 * 180) / (pi)

 alpha1.id <- which(alpha1 < 0)
 alpha1[alpha1.id] <- 2 * pi + alpha1[alpha1.id]
 Data2 <- subset(Data2, r > minR)
```

```
omega2<-Data2$omega
alpha2<-Data2$alpha
angvel2<-Data2$angvel
r2<-Data2$r
omega2<-omega2 - pi/2
alpha2<-alpha2 - pi/2
omega2.id <- which(omega2 < 0)
omega2[omega2.id] <- 2 * pi + omega2[omega2.id]
omega2<-(omega2 * 180) / (pi)

alpha2.id <- which(alpha2 < 0)
alpha2[alpha2.id] <- 2 * pi + alpha2[alpha2.id]

if (is.numeric(angvel1) & is.numeric(omega1)){
 Datadir1<- data.frame(angvel = angvel1,
                  omega = omega1, alpha = alpha1, r = r1)
 angvel = "angvel"
 omega = "omega"
 alpha = "alpha"
 r = "r"

 if (is.numeric(angvel2) & is.numeric(omega2)){
 Datadir2<- data.frame(angvel = angvel2,
                   omega = omega2, alpha = alpha2, r = r2)
 angvel = "angvel"
 omega = "omega"
 alpha = "alpha"
 r = "r"

 Datadir1$background<- 'Data1'
 Datadir2$background<- 'Data2'
 Datadir1$angvel[Datadir1$angvel==0] <- NA
 Datadir1$omega[Datadir1$omega==0] <- NA
```

```
Datadir2$angvel[Datadir2$angvel==0] <- NA

Datadir2$omega[Datadir2$omega==0] <- NA

Datadir1 <- na.omit(Datadir1)

Datadir2 <- na.omit(Datadir2)


Datadir<-rbind(Datadir1,Datadir2)

omega.breaks <- seq(0, 360, by = omegares)


omega.labels <- c(paste(seq(360-omegares, 0, by = -omegares),

                  "-",

                  seq(360, omegares, by = -omegares)))


omega.binned <- cut(Datadir[[omega]],

                breaks = omega.breaks,

                ordered_result = TRUE)

levels(omega.binned) <- omega.labels

Datadir$omega.binned <- omega.binned


angle_list <- unique(Datadir$omega.binned)


write.csv(Datadir,"K:/PhD/KV_recovery/Direction_graphs//Datadir.csv", row.names = FALSE)


for (i in seq_along(angle_list)) {

 Datasub<-subset(Datadir, Datadir$omega.binned==angle_list[i])

 # create plot for each anglebin in data

 plot <- ggplot(Datasub, aes(x=alpha, fill=background, color=background)) +

  ggtitle(angle_list[i]) +

  scale_fill_manual(values = c("#45D776", "#FF4747")) +

  scale_color_manual(values = c("#00C000", "#FF0000")) +

  coord_cartesian(ylim = c(0, 1)) +

  coord_polar(start = 3*pi/2, direction = -1) +

  geom_hline(yintercept = seq(0, 1, by = 0.25), colour = "white", size = 1) +

  geom_vline(xintercept = seq(0, 2*pi, by = pi/4), colour = "white", size = 1) +

  scale_x_continuous(limits = c(0,2*pi),
```

```
                labels = c("0 ", "90º",
                           "180º",
                           "270º",
                           "360º"),
                expand = c(0, 0),
                breaks = seq(0,2*pi, by = pi/2),
                minor_breaks = seq(0, 2*pi, by = pi/4)) +
    scale_y_continuous(limits = c(0,1)) +
    geom_histogram(aes(y=..density..), binwidth = pi/12, alpha= 0.8, position="identity", center = pi/24) +
          theme(panel.border = element_blank(),
        legend.key = element_blank(),
        panel.grid  = element_blank(),
        axis.text.x = element_text(color = "grey20", size = 20),
        axis.text.y = element_text(color = "grey20", size = 20),
        axis.title.y = element_text(color = "grey20", size = 20))
  print(plot)
  ggsave(plot, file=paste(results,
                  'Graphs_Statistics/',
                  angle_list[i], ".svg", sep=''), scale=2, bg = "transparent")
  kolmogrov.test<- with(Datasub, ks.test(alpha[background=="Data1"], alpha[background=="Data2"]))
  print (kolmogrov.test)

  capture.output(kolmogrov.test, file = paste(results,
                                 'Graphs_Statistics/',
                                 angle_list[i], ".txt", sep=''), append = TRUE)
  }
 }
}
}
```

S3 Statistical Linear Mixed Model for fluid extraction data (Relates to Figures 2d-g)

mdl =

Linear mixed-effects model fit by ML

Model information:
Number of observations 15775
Fixed effects coefficients 12
Random effects coefficients 69
Covariance parameters 7

Formula:
Linear Mixed Formula with 5 predictors.

Model fit statistics:

AIC	BIC
1961.5	2107.2

LogLikelihood	Deviance
-961.75	1923.5

Fixed effects coefficients (95% CIs):

Name	Estimate	SE	tStat	DF	pValue
{'(Intercept)' }	0.25153	0.022402	11.228	15763	3.8408e-29
{'Group_2' }	-0.032775	0.046137	-0.71037	15763	0.47748
{'Group_3' }	-0.12728	0.029113	-4.3719	15763	1.2396e-05
{'LR' }	0.0042934	0.0076882	0.55844	15763	0.57655
{'PA' }	0.16131	0.007627	21.15	15763	6.285e-98
{'Time' }	0.02145	0.0047745	4.4926	15763	7.0847e-06
{'Group_2:LR' }	0.026653	0.0097323	2.7387	15763	0.006176
{'Group_3:LR' }	-0.0026553	0.010254	-0.25896	15763	0.79567
{'Group_2:PA' }	0.033645	0.010982			
{'Group_3:PA' }	-0.041406	0.010603			
{'Group_2:Time'}	0.026635	0.0062842			
{'Group_3:Time'}	0.013497	0.0065969			

3.0635	15763	0.0021912
-3.905	15763	9.461e-05
4.2384	15763	2.2637e-05
2.0459	15763	0.040778

Lower	Upper
0.20762	0.29544
-0.12321	0.05766
-0.18434	-0.070215
-0.010776	0.019363
0.14636	0.17626
0.012091	0.030809
0.007577	0.04573
-0.022753	0.017443
0.012118	0.055171
-0.06219	-0.020622
0.014317	0.038953
0.00056621	0.026427

Random effects covariance parameters (95% CIs):
Group: EmbryoID (23 Levels)

Name1
{'(Intercept)'}
{'Group_2' }
{'Group_3' }
{'Group_2' }
{'Group_3' }
{'Group_3' }

Name2
{'(Intercept)'}
{'(Intercept)'}
{'(Intercept)'}
{'Group_2' }
{'Group_2' }
{'Group_3' }

Type	Estimate
{'std' }	0.052605
{'corr'}	-0.24831
{'corr'}	-0.85205
{'std' }	0.11948
{'corr'}	0.21158
{'std' }	0.074885

Lower	Upper
0.030563	0.090544
NaN	NaN
NaN	NaN
NaN	NaN
NaN	NaN
NaN	NaN

Group: Error

Name	Estimate
{'Res Std'}	0.25647

Lower Upper
0.25365 0.25931

S4 Statistical Linear Mixed Model for angular velocity dilution (DB) and viscosity (MC) experiments (relates to Figures 5c-f)

mdl =

Linear mixed-effects model fit by ML

Model information:
Number of observations 16622
Fixed effects coefficients 12
Random effects coefficients 90
Covariance parameters 7

Formula:
AAV ~ 1 + Intervention*LR + Intervention*PA + Intervention*Time + (1 + Intervention | EmbryoID)

Model fit statistics:
AIC BIC LogLikelihood Deviance
-4271.3 -4124.6 2154.6 -4309.3

Fixed effects coefficients (95% CIs):
Name Estimate SE tStat DF pValue Lower Upper
{'(Intercept)' } 0.25148 0.021717 11.58 16610 6.8705e-31 0.20891 0.29405
{'Intervention_2' } 0.070724 0.051808 1.3651 16610 0.17223 -0.030824 0.17227
{'Intervention_3' } -0.12344 0.035266 -3.5001 16610 0.00046626 -0.19256 -0.054311
{'LR' } 0.0042626 0.0063465 0.67164 16610 0.50182 -0.0081773 0.016702
{'PA' } 0.16135 0.0062961 25.626 16610 4.4137e-142 0.14901 0.17369
{'Time' } 0.021413 0.0039416 5.4325 16610 5.6349e-08 0.013687 0.029139
{'Intervention_2:LR' } -0.012356 0.0077958 -1.5849 16610 0.11301 -0.027636 0.002925
{'Intervention_3:LR' } 0.026366 0.009126 2.8891 16610 0.0038681 0.0084783 0.044254
{'Intervention_2:PA' } -0.02139 0.0079622 -2.6865 16610 0.0072282 -0.036997 -0.0057835
{'Intervention_3:PA' } -0.073208 0.0097269 -7.5263 16610 5.4857e-14 -0.092273 -0.054142
{'Intervention_2:Time'} -0.012635 0.0049043 -2.5763 16610 0.0099937 -0.022248 -0.0030222
{'Intervention_3:Time'} -0.0004407 0.0059861 -0.073621 16610 0.94131 -0.012174 0.011293

Random effects covariance parameters (95% CIs):
Group: EmbryoID (30 Levels)

	Name1	Name2	Type	Estimate	Lower	Upper
	{'(Intercept)' }	{'(Intercept)' }	{'std' }	0.052847	0.030895	0.090397
	{'Intervention_2'}	{'(Intercept)' }	{'corr'}	-0.2886	NaN	NaN
	{'Intervention_3'}	{'(Intercept)' }	{'corr'}	-0.96292	NaN	NaN
	{'Intervention_2'}	{'Intervention_2'}	{'std' }	0.16859	NaN	NaN
	{'Intervention_3'}	{'Intervention_2'}	{'corr'}	0.2779	NaN	NaN
	{'Intervention_3'}	{'Intervention_3'}	{'std' }	0.13252	NaN	NaN

Group: Error

Name	Estimate	Lower	Upper
{'Res Std'}	0.21169	0.20943	0.21398